AMERICAN JOURNAL OF PHYSIOLOGY
HEART AND CIRCULATORY PHYSIOLOGY

Am J Physiol Heart Circ Physiol 331: H669–H687, 2026.
First published July 9, 2026; doi:10.1152/ajpheart.00026.2026

RESEARCH ARTICLE

Women's Health Research and Novel Perspectives on Sex as an Investigative Variable

Potential role of tryptophan metabolites in the sex-based differences in doxorubicin-induced chronic cardiotoxicity in a rat model

Klaudia Kupecz,[1,2] Zsolt Galla,[3] Réka Losonczi,[1,2] Dávid Volford,[1,2] Andrea Siska,[4] Anita Sejben,[5] Moska Kohistani,[6] Merse Kis,[1,2] Réka Somogyi,[1,2] Zsombor András Greschik,[1] András Kriston,[7,8] Ferenc Kovács,[7,8] Péter Horváth,[7,8,9,10] Péter Bencsik,[6,11] Imre Földesi,[4] Péter Monostori,[3] Gábor Cserni,[5] Zsuzsanna Kahán,[12] and Márta Sárközy[1,2]

[1]*Cardiovascular Research Group, Department of Pathophysiology, Albert Szent-Györgyi Medical School, University of Szeged, Szeged, Hungary;* [2]*Department of Biochemistry, Albert Szent-Györgyi Medical School, University of Szeged, Szeged, Hungary;* [3]*Metabolic and Newborn Screening Laboratory, Department of Pediatrics, Albert Szent-Györgyi Medical School, University of Szeged, Szeged, Hungary;* [4]*Department of Laboratory Medicine, Albert Szent-Györgyi Medical School, University of Szeged, Szeged, Hungary;* [5]*Department of Pathology, Albert Szent-Györgyi Medical School, University of Szeged, Szeged, Hungary;* [6]*Department of Pharmacology and Pharmacotherapy, Albert Szent-Györgyi Medical School, University of Szeged, Szeged, Hungary;* [7]*Synthetic and Systems Biology Unit, Institute of Biochemistry, HUN-REN Biological Research Centre, Szeged, Hungary;* [8]*Single-Cell Technologies Ltd, Szeged, Hungary;* [9]*Institute for Molecular Medicine Finland, University of Helsinki, Helsinki, Finland;* [10]*Institute of AI for Health, Helmholtz Zentrum München, Neuherberg, Germany;* [11]*Pharmahungary Group, Szeged, Hungary; and* [12]*Department of Oncotherapy, Albert Szent-Györgyi Medical School, University of Szeged, Szeged, Hungary*

Abstract

The clinical use of doxorubicin (DOXO) may be limited by its dose-dependent chronic cardiotoxicity, the severity of which shows sex-based differences. Several tryptophan (Trp) metabolites are associated with oxidative stress, inflammation, and metabolic disturbances in heart failure. Here, we aimed to characterize changes in left ventricular (LV) concentrations of selected Trp metabolites in DOXO-induced chronic cardiotoxicity in both sexes. Therefore, male and female Wistar rats (300–400 g) were divided into 2-2 groups: physiological saline-treated (6 × 1 mL/kg, ip) control and DOXO-treated (6 × 1 mg/kg, ip) groups. At *weeks 12* and *19*, echocardiography was performed. At *week 20*, blood pressure measurement, histology in LV and renal samples, RT-qPCR, and ultra-high-performance liquid chromatography-tandem mass spectrometry (UHPLC-MS/MS) for genes and metabolites related to oxidative stress, inflammation, glucose and fatty acid metabolism, and Trp metabolites in LV samples were performed. At *week 12*, diastolic dysfunction developed in both sexes. At the endpoint, DOXO-treated animals showed echocardiographic, histological, and molecular signs of chronic cardiotoxicity, accompanied by LV repression of glycerol-3-phosphate dehydrogenase and carnitine palmitoyltransferase, overexpression of glucose transporter-1, increased levels of 3-hydroxykynurenine, and mild renal fibrosis without blood pressure elevation in both sexes. However, only male DOXO-treated rats exhibited systolic dysfunction, a lower reduced-to-oxidized glutathione ratio, overexpression of interleukin-6, increased levels of kynurenine, quinolinic acid, and glomerular hypertrophy. DOXO-treated females showed higher levels of anthranilic acid and overexpression of acyl-CoA dehydrogenase, suggesting better fatty acid utilization. In conclusion, male animals developed accelerated DOXO-induced chronic cardiotoxicity accompanied by more pronounced changes in the markers of oxidative stress, inflammation, and Trp metabolism.

NEW & NOTEWORTHY Doxorubicin (DOXO) induced accelerated chronic cardiotoxicity in males. In response to DOXO, both sexes developed mild renal fibrosis; however, only males showed histological signs of glomerular hypertrophy. Left ventricular concentrations of several tryptophan metabolites associated with oxidative stress and inflammation (kynurenine and quinolinic acid), metabolism (NAD^+), and fibrosis (indoxyl sulfate) were higher in DOXO-treated males. DOXO-treated females had higher left ventricular expression of acyl-CoA dehydrogenase, suggesting better fatty acid utilization.

doxorubicin; heart failure; kynurenine pathway; metabolic disturbances; sex-based differences

Correspondence: M. Sárközy (sarkozy.marta@med.u-szeged.hu).
Submitted 14 January 2026 / Revised 8 May 2026 / Accepted 2 July 2026

INTRODUCTION

Cancerous and cardiovascular diseases (CVDs) are the leading causes of death in high- and middle-income countries (1). Due to the recent diagnostic and therapeutic advances in oncology, long-term cancer survivors are one of the fastest-growing populations (2). After recurrent malignancies, CVDs are the second leading cause of morbidity and mortality in cancer survivors (3).

Anthracyclines, including DOXO, are effective and widely used chemotherapeutic agents in various cancer types, including leukemias and Hodgkin's lymphomas, as well as solid malignancies such as breast, ovarian, and lung cancers, in both pediatric and adult patients with cancer (4, 5). Although DOXO is one of the most potent antineoplastic agents, its clinical use might be limited by its dose-dependent side effects, including chronic cardiotoxicity characterized by dilated left ventricles with thinner walls and systolic and diastolic dysfunction (3, 6).

The underlying mechanisms of DOXO-induced chronic cardiotoxicity, particularly the sex-based differences, are multifactorial and have not yet been fully elucidated. Proposed mechanisms include cardiomyocyte (CM) membrane injury, DOXO-iron complex-catalyzed and cytochrome-P450-mediated free radical production leading to elevated oxidative stress, inflammatory mechanisms, mitochondrial damage, intracellular calcium overload, and various forms of cell death, including apoptosis, ferroptosis, and pyroptosis (4, 6–9). Notably, both clinical and preclinical studies reported sex-related differences in the development and severity of DOXO-induced chronic cardiotoxicity (5). In adult premenopausal patients and animal studies, female sex hormones might explain the less severe DOXO-induced cardiotoxicity in females by attenuating oxidative stress and apoptosis (5, 10). Indeed, in preclinical studies, the cardiac expression of several genes related to oxidative stress and cell death, as well as mitochondrial biogenesis and energy metabolism, has been shown to exhibit sexual dimorphism (5, 11, 12).

Nicotinamide adenine dinucleotide (NAD^+) serves as the primary electron carrier coenzyme in energy metabolism, such as glycolysis and the tricarboxylic acid cycle (13). It is a precursor to the de novo synthesis of $NADP^+$/NADPH, which plays a key role in anabolic reactions, the cellular redox state, and the glutathione (GSH) and thioredoxin antioxidant defense systems (14). Moreover, NAD^+/NADH serves as a cosubstrate for enzymes that play crucial roles in calcium homeostasis, DNA repair, cell survival, antioxidant defense, and metabolic regulation, such as cyclic ADP-ribose synthase, poly(ADP-ribose) polymerase (PARP), and sirtuins (13, 15). Declines in the NAD^+ level and altered NAD^+/NADH redox homeostasis have been reported in various CVDs, including heart failure (13).

NAD^+ is produced in the main Trp catabolic pathway, i.e., the kynurenine pathway (16). This pathway is increasingly recognized for its role in the development of heart failure; however, the pathophysiological roles of its metabolites, such as kynurenic acid and 3-hydroxykynurenine, remain controversial (17–20). Changes in several Trp metabolite levels, particularly kynurenine and quinolinic acid, are linked to oxidative stress, inflammation, immune responses, mitochondrial dysfunction, and metabolic shifts that can contribute to the development and progression of heart failure (17, 19, 21–25). Beyond NAD^+, these metabolites may represent additional targets for intervention in heart failure. However, their role and potential sex-dependent effects in DOXO-induced chronic cardiotoxicity have not been described yet.

Beyond the kynurenine pathway, Trp can be metabolized via the serotonin and indole pathways, producing a variety of biologically active metabolites (26). Although serotonin may increase contractility via 5-HT4 receptors in the heart as a compensatory mechanism, long-term elevation can contribute to the progression of heart failure by altering calcium handling and activating fibroblasts (27). Moreover, indoxyl sulfate (INS), a well-known uremic toxin produced by the gut microbiota and liver, is associated with heart failure and cardiovascular events in patients with chronic kidney disease via various mechanisms, including oxidative stress, inflammation, and fibrosis in the heart (28). In contrast, indole-3-propionic acid has been shown to attenuate diastolic dysfunction, metabolic remodeling, oxidative stress, and inflammation while also restoring NAD^+/NADH and sirtuin levels in heart failure with preserved ejection fraction (EF; 29).

Therefore, in our present study, we aimed to characterize changes in LV concentrations of selected Trp metabolites across the kynurenine, serotonin, and indole pathways in a rat model of DOXO-induced chronic cardiotoxicity in both sexes.

MATERIALS AND METHODS

Ethics Approval

This investigation conformed to the EU Directive 2010/63/EU. It was approved by the regional Animal Research Ethics Committee of Csongrad County (project license X./462/2024, dated March 26, 2024) and by the University of Szeged in Hungary. All institutional and national guidelines for the care and use of laboratory animals were followed.

Animals

A total of 16 male (300–400 g) and 18 female (200–260 g) Wistar Hannover rats (*Rattus norvegicus*, strain: HanTac: WH, RRID: RGD_1566433, 8–10 wk old, Charles-Rivers Laboratories, Germany) were housed in individually ventilated cages (Tecniplast Sealsafe IVC system, Buguggiate, Italy) under a 12/12-h light/dark cycle in a temperature-controlled room (22 ± 2°C; relative humidity 55% ± 10%) with access to standard rat chow and tap water ad libitum.

Experimental Setup

After 1 wk of acclimatization, male and female animals were randomized into two control and two DOXO-treated groups based on body weight ($n = 7$–9 animals; Fig. 1). At *days 1*, *4*, *7*, *10*, *13*, and *16*, control rats were treated with saline (1 mL/kg, ip) and animals in the DOXO group were administered DOXO (1 mg/kg, ip; Doxorubicin Teva 2 mg/mL, Teva Pharmaceutical Industries Ltd., Debrecen, Hungary, i.e., 6 mg/kg cumulative dose; Fig. 1). The dosing and timing of DOXO cycles were calculated based on preclinical studies and

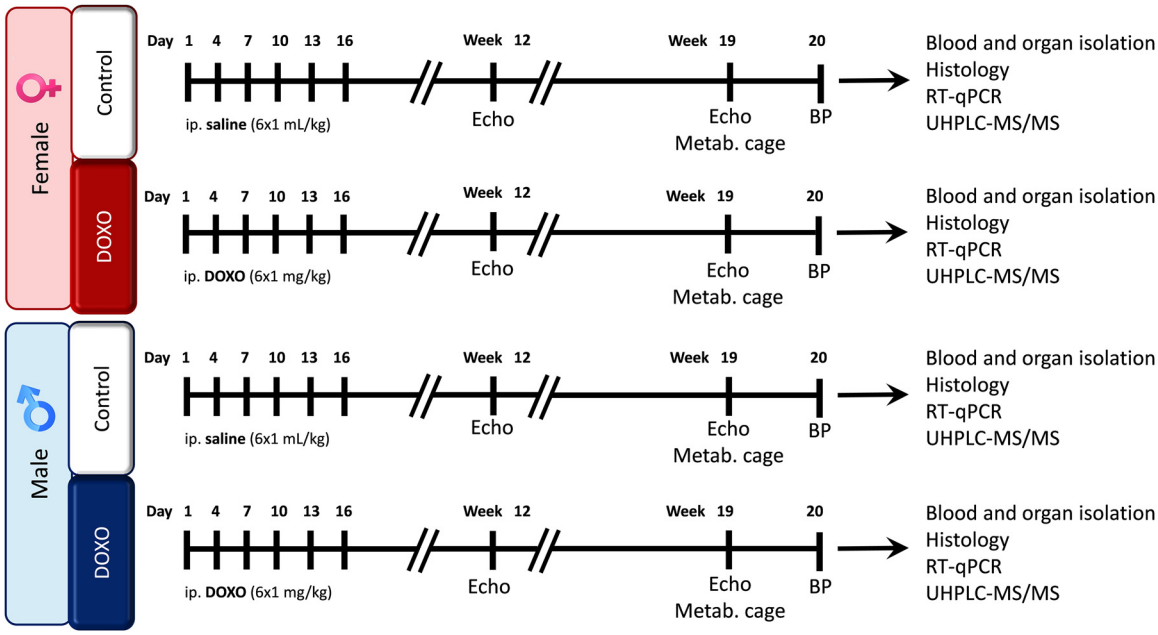

Figure 1. Experimental setup. Male and female Wistar rats were divided into 2-2 groups: control treated with physiological saline (6 × 1 mL/kg, ip), and DOXO (6 × 1 mg/kg, ip) groups. The animals were then followed for 20 wk. At *weeks 12* and *19*, echocardiography was performed to assess cardiac function and morphology. At *week 19*, the animals were placed into metabolic cages for 24 h to collect urine. At *week 20*, arterial blood pressure (BP) measurement was performed under anesthesia. Then, blood was collected from the abdominal aorta, and hearts, lungs, kidneys, and tibias were isolated. Histopathological examinations were performed on left ventricular and kidney samples to assess fibrosis and hypertrophy. Real-time quantitative polymerase chain reaction (RT-qPCR) was performed to quantify gene expression related to nitro-oxidative stress, inflammation, glucose, and fatty acid metabolism. Ultra-high-performance liquid chromatography-tandem mass spectrometry (UHPLC-MS/MS) was used to measure oxidative stress markers, Trp, and glucose metabolites. DOXO, doxorubicin; Trp, tryptophan.

human chemotherapy regimens, adjusted for rat metabolism and body surface area (30–33). At *weeks 12* and *19*, echocardiography was performed to assess cardiac morphology and function. Then, animals were placed in metabolic cages (Tecniplast Metabolic Cage System, Buguggiate, Italy) for 24 h to collect urine. At *week 20*, blood pressure was measured under isoflurane anesthesia (Forane, Aesica, Queenborough Limited, Queenborough, UK). Thereafter, the abdominal cavity was opened to collect blood from the aorta. Then, rats were euthanized by overdosing on sodium pentobarbital (100 mg/kg, ip). The hearts, lungs, kidneys, and tibias were excised and washed in Krebs–Henseleit solution to remove blood. The total heart, LV, right ventricular, kidney, and lung weights were measured, and the left ventricles were transversely sectioned from the mid-papillary to the basal level. The basal parts of the left ventricles and the mid parts of the left kidney were fixed in 4% buffered formalin for histological analysis. The apical parts of the left ventricles were freshly frozen in liquid nitrogen and stored at −80°C until further biochemical measurements, including RT-qPCR and ultra-high-performance liquid chromatography-tandem mass spectrometry (UHPLC-MS/MS, Fig. 1).

Transthoracic Echocardiography

At *weeks 12* and *19*, cardiac morphology and function were assessed by TTE, as previously described (34, 35). In brief, rats were anesthetized with 2% isoflurane (Forane, Aesica, Queenborough Limited, Queenborough, UK). Two-dimensional (2D) B-mode, M-mode in the parasternal long-axis view, pulsed-wave Doppler, and tissue Doppler images were performed by the criteria of the American Society of Echocardiography with a Vivid IQ ultrasound system (General Electric Medical Systems, New York, NY) using a phased array 5.0–11 MHz transducer (General Electric 12S-RS probe, General Electric Medical Systems, New York, NY). Data from three consecutive heart cycles were analyzed (EchoPAC Dimension v201, General Electric Medical Systems) by an experienced investigator in a blinded manner. The mean values of three measurements were calculated and used for statistical evaluation. Systolic and diastolic septal and posterior wall thicknesses (SWTs, SWTd, PWTs, and PWTd, respectively) were obtained from the parasternal long-axis view at the level of the mitral valve. The left ventricular internal diameters at the end of systole and diastole (LVESD and LVEDD) were measured by M-mode echocardiography from the long-axis view between the endocardial borders. The LV relative wall thickness was calculated as (2 × PWTd)/LVEDD. Isovolumic contraction time (IVCT), ejection time (ET), and isovolumic relaxation time (IVRT) were measured using pulsed-wave Doppler across the mitral valve. IVCT was measured as the time from mitral valve closure to aortic valve opening. ET was determined as the time from aortic valve opening to aortic valve closure. IVRT was defined as the time from aortic valve closure to mitral valve opening. The myocardial performance (Tei) index was calculated as (IVCT + IVRT)/ET. The left ventricular end-diastolic volume (LVEDV) and left ventricular end-systolic volume (LVESV) were calculated on two-dimensional four-chamber view images delineating the endocardial borders in diastole and systole. The stroke volume (SV) was calculated as the difference between LVEDV and LVESV. Ejection fraction (EF) was calculated using the

formula (SV/LVEDV) × 100. Cardiac output (CO) was calculated as the product of SV and heart rate (HR).

Blood Pressure Measurements

At *week 20*, animals were anesthetized with isoflurane (induction 5% and maintenance 2%) in the presence of room air with a flow of 2 L/min, and placed onto a homeothermic blanket (Thermostar Model 69020, RWD Life Science Co, Ltd.) to control and maintain body core temperature (at 36.5°C ± 1.0°C). A median incision was made on the neck, and the right common carotid artery was isolated and separated from the vagal nerve. The cranial end of the isolated section was ligated with a Mersilk 5-0 thread (Ethicon, Johnson & Johnson Ltd., Budapest, Hungary), and a loop was placed under the aboral portion of the vessel. A small incision was made in the arterial wall near the cranial ligature, and a PE50 polyethylene catheter (BTPE-25, Instech Laboratories, Inc., Plymouth, PA) was inserted into the artery. Blood pressure measurements were performed between 08:30 AM and 2:00 PM using a SEN-02 pressure transducer (MDE Medical Biology Research, Development, and Manufacturing Ltd., Budapest, Hungary) connected to an EXP-HG-1 amplifier (MDE Ltd.) and aWS-DA data acquisition system (MDE Ltd.). Data were recorded, and blood pressure was evaluated using S.P.E.L. Advanced Haemosys software (MDE Ltd.). A short time (3–4 min) after equilibration and stabilization of hemodynamic parameters following cannulation, a 50-s segment of blood pressure and ECG recordings was evaluated to obtain heart rate and systolic, diastolic, and mean arterial blood pressure values. The average of the 50 s recordings at 2 kHz was used to compare blood pressure values across different study groups.

Urine Laboratory Parameters

Urine creatinine and protein levels were determined to assess the toxic effects of DOXO on the kidneys. Urine creatinine and urine protein levels were measured by standard laboratory methods as described previously (35, 36).

Serum Laboratory Parameters

Serum albumin concentration was measured by a colorimetric assay (Hoffmann-La Roche Ltd., Switzerland) using bromocresol green as an anionic dye that binds to albumin. The color intensity of the blue-green color is directly proportional to the albumin concentration in the sample and is measured photometrically.

Serum urea and creatinine levels were quantified using a kinetic UV spectrophotometric method, following Jaffe's method as previously described (35, 36). The reagents and the platform analyzers were from Roche Diagnostics (Hoffmann-La Roche Ltd., Switzerland).

Creatinine clearance was calculated according to the standard formula [urine creatinine concentration (μM) × urine volume for 24 h (mL)]/[serum creatinine concentration (μmol/L) × 24 × 60 min] (35, 36). Urine volume and urine creatinine concentrations were measured at *week 19*.

Serum glucose levels were quantified using the hexokinase enzymatic method as a reference. During the reaction, the rate of NADPH formation is directly proportional to the glucose concentration and is measured photometrically.

Serum total cholesterol, high-density lipoprotein (HDL) cholesterol, and triglyceride levels were measured using the Roche Cobas 8000 analyzer system and enzymatic colorimetric assays from Roche (Hoffmann-La Roche Ltd., Switzerland; 37). Low-density lipoprotein (LDL) cholesterol was calculated according to the Friedewald formula (37).

Histological Analyses

Subvalvular areas of the left ventricles were fixed in formalin, embedded in paraffin, cut transversally into 5-μm sections, and stained with hematoxylin-eosin (HE) or picrosirius red/fast green (PSFG), as described previously (35, 38). Histological slides were scanned with a Pannoramic Midi II scanner (3-D-Histech, Budapest, Hungary). Digital slide processing was performed using SlideViewer version 2.6 (last accessed August 14, 2024).

On the digital HE images, cardiomyocyte (CM) perimeters and cross-sectional areas were evaluated using the Biology Image Analysis Software (BIAS 1.0, Single-Cell Technologies Ltd., Szeged, Hungary, https://single-cell-technologies.com/bias/) (35, 38). Glomerular and tubular diameters were measured on HE-stained kidney sections using digital slides, and the largest diameters were recorded for each. Fifty glomeruli and tubules per animal were randomly selected for analysis. LV and renal fibrosis were assessed on PSFG slides using an in-house-developed program as described previously (34, 35, 38). Representative HE- and PSFG-stained slides were captured in Panoramic Viewer 1.15.4 (3-D-Histech, Budapest, Hungary; https://old.3dhistech.com/pannoramic_viewer).

Transcription Profiling by Quantitative Reverse Transcription Polymerase Chain Reaction in Left Ventricular Tissue Samples

Quantitative RT-PCR was performed using gene-specific primers to monitor LV mRNA expression, as previously described (34, 38). Qiagen RNeasy Fibrous Tissue Mini Kit (Qiagen, Hilden, Germany) was used to isolate RNA. It was quantified using a NanoDrop One Microvolume UV-Vis spectrophotometer (Thermo Fisher Scientific Inc., Waltham, MA). Then, 100 μg of total RNA was reverse-transcribed using the iScript cDNA synthesis kit (Bio-Rad Laboratories Inc., Hercules, CA). The cDNAs were analyzed in technical duplicates using 10 μL reaction volumes. Specific primers (*Acadl*: long-chain specific acyl-CoA dehydrogenase, mitochondrial, No. qRnoCIP0029670; *Acox1*: peroxisomal acyl-coenzyme A oxidase 1, No. qRnoCIP0027493; *Aldoa*: aldolase A, No. qRnoCED0001360; *Cpt1a*: carnitine *O*-palmitoyltransferase 1, liver isoform, No. qRnoCIP0031435; *Gapdh*: glyceraldehyde-3-phosphate dehydrogenase, No. qRnoCID0057018; *Il6:* interleukin-6, No. qRnoCID0053166; *Ldha*: lactate dehydrogenase A chain, No. qRnoCED0006780; *Myh6*: α-myosin heavy chain, No. qRnoCID0001766; *Myh7*: β-myosin heavy chain, No. qRnoCED0001215; *Nppa*: A-type natriuretic peptide, No. qRnoCED0006216; *Pfk:* 6-phosphofructokinase, liver type, No. qRnoCID0001033; *Pkm*: pyruvate kinase isozymes M1/M2, No. qRnoCID0002639; *Slc2a1:* solute carrier family 2 member 1, No. qRnoCEP0025043 and *Slc2a4:* solute carrier family 2 member 4, No. qRnoCIP0023827) and SsoAdvanced Universal SYBR Green Supermix (all from BioRad Laboratories Inc., Hercules, CA) were applied

according to the manufacturer's instructions using a BioRad CFX-96 machine and BioRad CFX Manager software (BioRad Laboratories Inc., Hercules, CA) for cycle threshold value analysis. Gene expression was calculated using the relative standard curve method. Ubiquitin C (*Ubc*, No. qRnoCED0057022, BioRad Laboratories Inc., Hercules, CA) was used as a housekeeping control gene for normalization.

Left Ventricular Metabolite Measurements by UHPLC-MS/MS

The LV samples were prepared, and metabolite levels were quantified by ultra-high-performance liquid chromatography-tandem mass spectrometry (UHPLC-MS/MS). Sample preparation and chromatographic conditions were applied as described in our previously published protocols (39–41). Although mass spectrometric parameters (i.e., MRM transitions, declustering potentials, and collision energies) and retention times were previously reported for several analytes (39–41), they were not consistently detailed for all compounds measured in the present work. Therefore, the missing MS settings and retention times used in this study are provided in the next paragraph to ensure complete transparency and reproducibility.

MRM transition of indoxyl sulfate (INS) was 211.9/131.9 using −50 V as the declustering potential and −25 V as the collision energy; retention time: 11.48 min. MRM transition of asymmetric dimethyl arginine (ADMA) was 203.2/46.0 using 50 V as the declustering potential and 30 V as the collision energy; retention time: 1.00 min. MRM transition of symmetric dimethyl arginine (SDMA) was 203.2/172.0 using 50 V as the declustering potential and 20 V as the collision energy; retention time: 1.06 min. MRM transition of reduced glutathione (GSH) was 308.2/179.1 using 50 V as the declustering potential and 14 V as the collision energy; retention time: 1.76 min. MRM transition of oxidized glutathione (GSSG) was 614.4/485.1 using 50 V as the declustering potential and 17 V as the collision energy; retention time: 2.58 min. MRM transition of NAD^+ was 664.2/136.1 using 85 V as the declustering potential and 50 V as the collision energy; retention time: 2.00 min. MRM transition of lactate was 88.9/43.0 using −50 V as the declustering potential and −15 V as the collision energy; retention time: 1.70 min. MRM transition of pyruvate was 86.9/59.0 using −50 V as the declustering potential and −11 V as the collision energy; retention time: 1.30 min. MRM transition of indole-3-lactic acid was 206.1/188.1 using 50 V as the declustering potential and 12 V as the collision energy; retention time: 13.00 min. MRM transition of indole-3-propionic acid was 190.1/130.1 using 50 V as the declustering potential and 19 V as the collision energy; retention time: 13.00 min. MRM transition of indole-3-carboxaldehyde was 146.1/118.1 using 50 V as the declustering potential and 19 V as the collision energy; retention time: 12.40 min.

Statistical Analysis

The sample size was calculated using the freely available sample size calculator software G*Power (RRID: SCR_013726, version 3.1.9.7, downloaded from https://www.psychologie.hhu.de/arbeitsgruppen/allgemeine-psychologie-und-arbeitspsychologie/gpower). All statistical analyses were performed with GraphPad Prism Software (RRID: SCR_002798, version 8.01, GraphPad Software Inc., Boston, MA). The normal distribution of the data was assessed using the Shapiro–Wilk test. Two-way analysis of variance (ANOVA) was used to compare groups. In cases of significant differences between groups, multiple pairwise comparisons were corrected for multiple comparisons using the Holm–Sidak method in the post hoc test. All values are presented as means ± SE, and a P value of <0.05 was accepted as statistically significant.

RESULTS

DOXO Treatment Resulted in More Severe Renal Dysfunction in Males

Because of the toxic effects of DOXO on the kidneys and the crosstalk between cardiac and renal function, kidney function parameters were assessed at the end point (Table 1). Both males and females showed significantly lower serum albumin levels and higher urinary protein concentrations in response to DOXO treatment than their sex-matched controls (Table 1). However, DOXO-treated females had significantly higher serum albumin levels than DOXO-treated males (Table 1). Moreover, DOXO-treated males showed markedly higher serum urea and creatinine concentrations and a tendency toward decreased creatinine clearance ($P = 0.053$) compared with the sex-matched control group (Table 1). There were no marked differences in the urine volume among the groups (Table 1).

DOXO-Treated Males Developed Heart Failure at an Accelerated Rate Based on Echocardiography

Transthoracic echocardiography was performed at *weeks 12* and *19* to investigate whether DOXO leads to similar LV morphological and functional alterations in both sexes (Supplemental Figs. S1–S3, Fig. 2, *A–H* and Fig. 3, *A–F*).

Table 1. *The effects of sex and DOXO on serum and urine parameters*

Parameter (Unit)	Control Male	DOXO Male	Control Female	DOXO Female
Serum albumin, g/L	37 ± 0.7	26 ± 1.9*	43 ± 0.9#	38 ± 1.5*#
Urine protein, mg/dL	93 ± 55	1,116 ± 358*	67 ± 12	531 ± 144
Serum urea, mmol/L	6.9 ± 0.4	8.5 ± 0.6*	7.6 ± 0.4	8.0 ± 0.4
Serum creatinine, μmol/L	39 ± 1.9	54 ± 5.7*	38 ± 2.9	41 ± 3#
Urine creatinine, μmol/L	4,865 ± 823	5,343 ± 649	4,254 ± 394	2,592 ± 316*#
Urine volume, mL	31 ± 4.23	28 ± 2.68	28 ± 5.81	35 ± 5.54
Creatinine clearance	2.12 ± 0.15	1.53 ± 0.21	1.46 ± 0.09#	1.25 ± 0.1

Values are presented as means ± SE. DOXO, doxorubicin. *$P < 0.05$ DOXO vs. control group, #$P < 0.05$ females vs. males ($n = 7$–9 animals, one-way ANOVA, Holm–Sidak post hoc test).

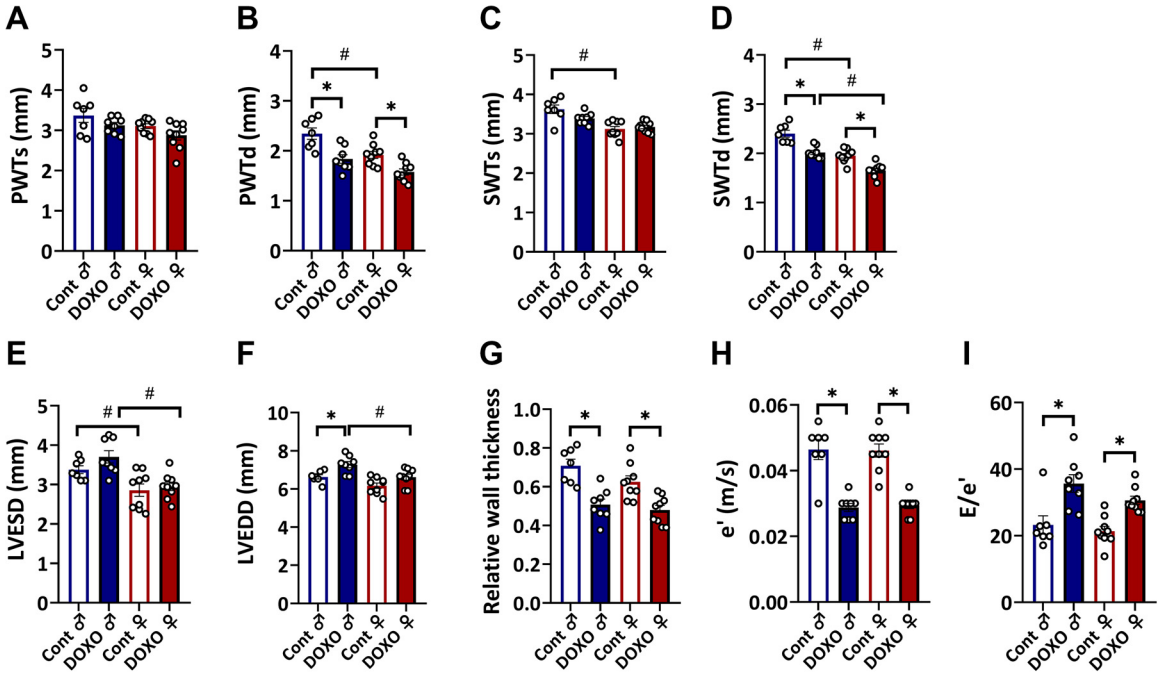

Figure 2. The effects of sex and DOXO on echocardiographic parameters at *week 19*. *A*: posterior wall thicknesses in systole (PWTs), posterior wall thicknesses in diastole (PWTd, *B*), septal wall thicknesses in systole (SWTs, *C*), septal wall thicknesses in diastole (SWTd, *D*), left ventricular end-systolic diameter (LVESD, *E*), left ventricular end-diastolic diameter (LVEDD, *F*), relative wall thickness calculated as (2 × PWTd)/LVEDD (*G*), early diastolic mitral annular velocity (e′, *H*), and ratio of the peak early diastolic mitral inflow velocity to the early diastolic mitral annular velocity (E/e′, *I*). Values are presented as means ± SE, $*P < 0.05$ DOXO vs. control group, $\#P < 0.05$ females vs. males ($n = 7$–9 animals, one-way ANOVA, Holm–Sidak post hoc test). Cont, control; DOXO, doxorubicin.

At *week 12*, posterior and septal wall thicknesses, LV diameters and volumes, as well as CO, were significantly lower in females independent of DOXO treatment due to their smaller body size compared with males (Supplemental Figs. S1 and S2). However, at this stage, there were no significant differences in LV wall thicknesses, diameters, relative wall thickness, volumes, or EF between the control and DOXO-treated groups in either sex (Supplemental Figs. S1–S3). Notably, the e′ was significantly lower and the E/e′ was markedly higher only in the male DOXO-treated group compared with the male control group, indicating echocardiographic signs of diastolic dysfunction (Supplemental Fig. S1). There were no significant differences in IVRT, IVCT, ET, and Tei index among the groups at *week 12* (Supplemental Fig. S3, *A* and *D*).

At *week 19*, PWTd and SWTd, as well as LVESD, were significantly decreased in control females compared with the control males, due to the smaller body size of females (Fig. 2, *B*, *D*, and *E*). In response to DOXO treatment, both sexes showed markedly reduced PWTd and SWTd, as well as decreased relative wall thickness, compared with the sex-matched control groups (Fig. 2, *B*, *D*, and *G*). However, only the DOXO-treated males showed a significantly increased LVEDD, LVESV, LVEDV, SV, and CO, as well as markedly decreased EF compared with the male control group, indicating the development of LV dilation at an accelerated rate in DOXO-treated males (Fig. 2*G*, Fig. 3, *A*–*C*, *E*, and *F*). The heart rate tended to increase in the DOXO-treated males ($P = 0.051$) as compared with the sex-matched control group (Fig. 3*D*). In the DOXO-treated females, LVESV ($P = 0.055$) and EF ($P = 0.087$) tended to increase (Fig. 3, *B* and *F*). Both DOXO-treated males and females developed diastolic dysfunction, indicated by markedly reduced e′ and elevated E/e′, as well as shorter IVRT compared with the sex-matched control groups (Fig. 3, *G* and *H*, Supplemental Fig. 3*E*). There were no significant differences in the IVCT, ET, and Tei index among the groups at *week 19* (Supplemental Fig. S3, *F*–*H*). Moreover, blood pressure values, including systolic, diastolic, and mean arterial pressures, did not differ significantly from those measured in the control animals at *week 20* (Fig. 3, *G*–*I*).

DOXO Treatment Led to Reduced Heart Weight and Increased Kidney Weight in Males Only

Females had significantly lower body weights at both the start and the end of the experiment than males (Table 2). Due to their smaller body size, females had lower organ weights, including the heart, left and right ventricles, lungs, and kidneys, as well as shorter tibia length (Table 2). In response to DOXO treatment, males showed lower heart and LV weights and increased kidney weight than females, consistent with laboratory and echocardiographic results (Table 2).

Both Sexes Showed Histological Signs of Compensatory Cardiomyocyte Hypertrophy and Interstitial Fibrosis in Response to DOXO Treatment

CM cross-sectional areas were measured on HE-stained slides to observe the cardiac effects of DOXO at the cellular level (Fig. 4*A*). CM cross-sectional areas were significantly increased in both DOXO-treated groups compared with the sex-matched control groups, suggesting the development of

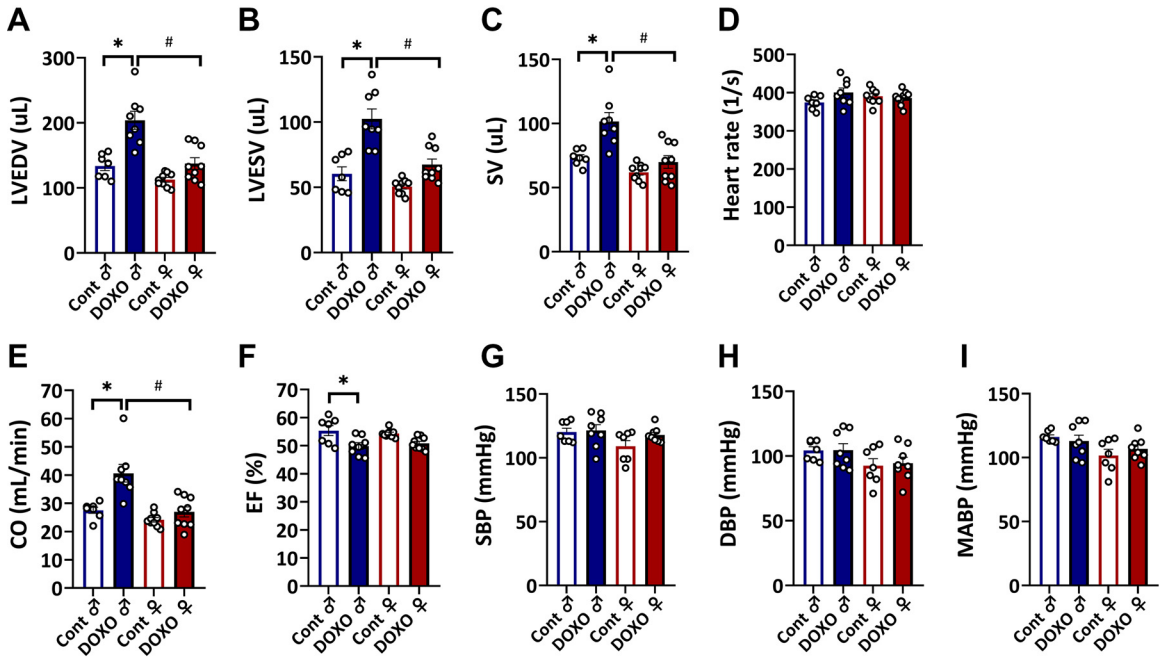

Figure 3. The effects of sex and DOXO on hemodynamic parameters measured by echocardiography at the endpoint. *A*: left ventricular end-diastolic volume (LVEDV), left ventricular end-systolic volume (LVESV, *B*), stroke volume (SV, *C*), heart rate (HR, *D*), cardiac output (CO, *E*), ejection fraction (EF, *F*), systolic blood pressure (SBP, *G*), diastolic blood pressure (DBP, *H*), and mean arterial blood pressure (*I*). Values are presented as means ± SE, $*P < 0.05$ DOXO vs. control group, $\#P < 0.05$ females vs. males ($n = 6$–9 animals, one-way ANOVA, Holm–Sidak post hoc test). Cont, control; DOXO, doxorubicin.

compensatory hypertrophy in the surviving CMs (Fig. 4*B*). To strengthen our results on CM hypertrophy, the ratio of LV expression of the myosin heavy chain β (*Myh7*) and α (*Myh6*) isoforms was measured as a molecular marker of hypertrophy. The *Myh7/Myh6* ratio tended to increase ($P = 0.051$) only in DOXO-treated males compared with the sex-matched control group (Fig. 4*C*). PSFG-stained slides were used to assess LV fibrosis development (Fig. 4*A*). The LV collagen content was significantly increased in both sexes in response to DOXO treatment compared with the sex-matched control groups, confirming the development of LV interstitial fibrosis (Fig. 4*D*).

Both Sexes Developed Mild Renal Fibrosis, and Only Males Showed Glomerular Hypertrophy in Response to DOXO Treatment

Glomerular and tubular diameters were measured on HE-stained slides, and renal fibrosis was assessed on PSFG-stained slides (Supplemental Fig. S4, *A*–*C*). Only DOXO-treated males showed significantly increased glomerular diameters compared with the sex-matched control group (Supplemental Fig. S4*A*). There were no significant differences in the tubular diameters among the groups (Supplemental Fig. S4*B*). In response to DOXO, both sexes developed mild renal fibrosis compared with the sex-matched control group (Supplemental Fig. S4*C*).

DOXO Treatment Resulted in Left Ventricular Overexpression of Inflammatory and Oxidative Stress Markers in Males

The myocardial stretch marker *Nppa* and the inflammatory marker *Il6* were significantly overexpressed only in the male DOXO-treated animals compared with the sex-matched controls (Fig. 5, *A* and *B*). In accordance with the echocardiographic results, the LV *Nppa* expression tended to increase ($P = 0.065$) in the female DOXO-treated group compared with the female control group, and it was markedly lower compared with the male DOXO-treated group (Fig. 5*B*). The ratio of the reduced and oxidized glutathione (GSH/GSSG) was significantly lower in the DOXO-treated male group

Table 2. *The effects of sex and DOXO on body weights and organ weights*

Parameter (Unit)	Control Male	DOXO Male	Control Female	DOXO Female
Body weight at the beginning, g	343 ± 16	351 ± 8	230 ± 5#	228 ± 5#
Body weight at the endpoint, g	490 ± 23	442 ± 13	289 ± 11#	280 ± 10#
Heart weight, mg	1,081 ± 62	974 ± 22*	733 ± 8#	739 ± 12#
Left ventricle weight, mg	876 ± 41	787 ± 27*	599 ± 10#	599 ± 9#
Right ventricle weight, mg	189 ± 27	168 ± 9	126 ± 8#	144 ± 6
Lung weight, g	1,515 ± 46	1,523 ± 33	1,158 ± 23#	1,151 ± 28#
Kidney weight, g	1,273 ± 73	1,737 ± 141*	833 ± 26#	917 ± 44#
Tibia length, cm	42 ± 0.33	42 ± 0.26	38 ± 0.5#	39 ± 0.29#

Values are presented as means ± SE. DOXO, doxorubicin. $*P < 0.05$ DOXO vs. control group, $\#P < 0.05$ females vs. males ($n = 7$–9 animals, one-way ANOVA, Holm–Sidak post hoc test).

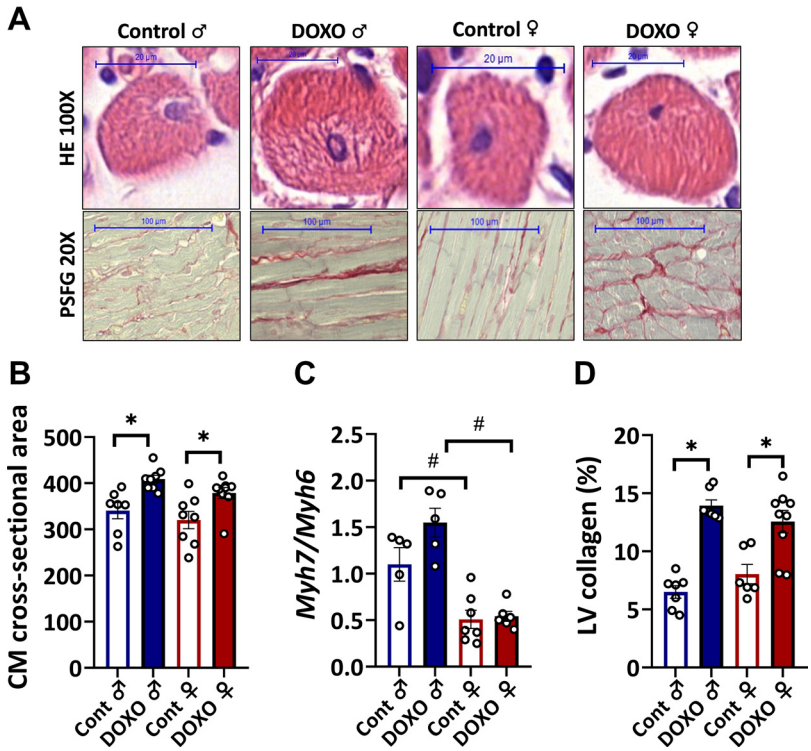

Figure 4. The effects of sex and DOXO on cardiomyocyte hypertrophy and interstitial fibrosis. *A*: representative histological sections stained with hematoxylin-eosin (HE, 100×) and picrosirius red and fast green (PSFG, 20×), cardiomyocyte (CM) cross-sectional area (μm^2) (*B*), β-myosin heavy chain to α-myosin heavy chain ratio (Myh7/Myh6) (*C*), and left ventricular (LV) collagen content (*D*). Values are presented as means ± SE, $^*P < 0.05$ DOXO vs. control group, $\#P < 0.05$ females vs. males (n = 5–9 animals, one-way ANOVA, Holm–Sidak post hoc test). Cont, control; DOXO, doxorubicin.

only, and it tended to decrease in the female DOXO-treated group ($P = 0.10$) compared with the sex-matched control groups, indicating elevated LV oxidative stress (Fig. 5*C*). LV endothelial nitric oxide synthase (*Nos3*) was significantly repressed in both DOXO-treated groups, suggesting LV remodeling in both sexes (Fig. 5*D*). However, the LV *Nos3* expression was markedly lower in females independently of DOXO treatment (Fig. 5*D*). The LV concentrations of the endothelial nitric oxide synthase (eNOS) inhibitors ADMA and SDMA were markedly increased in the DOXO-treated males compared with the sex-matched controls, probably contributing to the elevated oxidative stress and accelerated heart failure in the DOXO-treated males (Fig. 5, *E* and *F*). In addition, the LV level of the Trp metabolite and uremic toxin indoxyl sulfate was markedly higher only in the DOXO-treated males compared with control males (Fig. 5*G*).

Left Ventricular Kynurenic Acid and NAD^+ Concentrations Were Higher in DOXO-Treated Males

There were no significant differences in the LV Trp levels between the groups (Fig. 6*A*). In response to DOXO treatment, LV kynurenine levels were significantly higher in males than in sex-matched controls (Fig. 6*B*). In addition, DOXO-treated females had markedly lower kynurenine levels than DOXO-treated males (Fig. 6*B*). LV kynurenic acid concentrations were not significantly different between the DOXO-treated and sex-matched control groups (males, $P = 0.12$; females, $P = 0.22$, Fig. 6*C*). The LV anthranilic acid concentrations were significantly elevated only in the DOXO-treated female rats compared with the sex-matched control group (Fig. 6*D*). In addition, the female DOXO-treated group had a markedly elevated anthranilic acid level compared with that in the male DOXO-treated group (Fig. 6*D*). In response to DOXO treatment, LV 3-hydroxykynurenine concentrations were markedly higher in both sexes than in the sex-matched control groups (Fig. 6*E*). There were no significant differences in the LV xanthurenic acid levels between the groups (Fig. 6*F*). The DOXO-treated males showed markedly elevated LV quinolinic acid concentrations compared with the sex-matched control group (Fig. 6*G*). The LV quinolinic acid levels were slightly higher ($P = 0.12$) in the female DOXO-treated group compared with the sex-matched control group (Fig. 6*G*). Interestingly, NAD^+ concentration was significantly elevated only in the male DOXO-treated group compared with the sex-matched control group (females, $P = 0.37$; Fig. 6*H*). In addition, the DOXO-treated females had markedly lower LV NAD^+ levels than DOXO-treated males (Fig. 6*H*).

The LV concentrations of additional Trp metabolites, including serotonin, 5-hydroxyindoleacetic acid, indole-3-acetic acid, indole-3-propionic acid, and indole-3-lactic acid, were not significantly different between the groups (Fig. 7, *A*–*E*). The indole-3-carboxaldehyde level was markedly elevated only in the DOXO-treated males compared with the sex-matched control group (Fig. 7*F*).

DOXO Alters the Expression of Genes Associated with Glucose Uptake and Glycolysis in the Left Ventricle in Both Sexes

There was no significant difference in the serum glucose levels between the groups (Fig. 8*A*). The insulin-independent glucose transporter 1 (*Slc2a1*) was markedly overexpressed, and the insulin-dependent glucose transporter 4 (*Slc2a4*) was significantly repressed in the left ventricles of the DOXO-treated groups as compared with those of the sex-matched control groups (Fig. 8, *B* and *C*). The LV expression of aldolase-A (*Aldoa*), responsible for the conversion of fructose-1,6-bisphosphate to glyceraldehyde 3-phosphate during

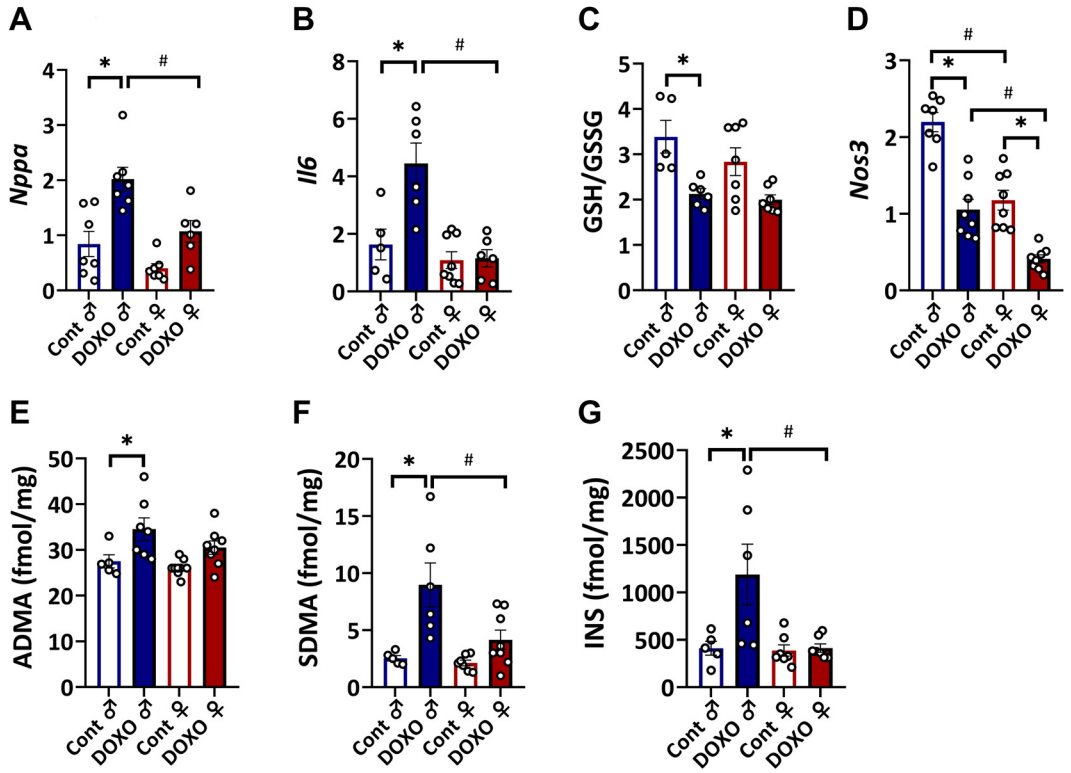

Figure 5. The effects of sex and DOXO on left ventricular gene expression and metabolite concentrations related to myocardial stretch, nitro-oxidative stress, and inflammation. A-type natriuretic peptide (*Nppa*; *A*), interleukin-6 (*Il6*, *B*), reduced glutathione to oxidized glutathione ratio (GSH/GSSG, *C*), endothelial nitric oxide synthase (*Nos3*, *D*), asymmetric dimethylarginine (ADMA, *E*), symmetric dimethylarginine (SDMA, *F*), and indoxyl sulfate (INS, *G*). Values are presented as means ± SE, $*P < 0.05$ DOXO vs. control group, $\#P < 0.05$ females vs. males ($n = 5$–9 animals, one-way ANOVA, Holm–Sidak post hoc test). Cont, control; DOXO, doxorubicin.

glycolysis, was significantly lower in both DOXO-treated groups compared with the sex-matched control groups (Fig. 8*D*). Importantly, the NAD^+-using enzyme in glycolysis, i.e., glyceraldehyde-3-phosphate dehydrogenase (*Gapdh*), was markedly repressed in the left ventricles of both DOXO-treated groups as compared with that in the sex-matched control groups (Fig. 8*E*). In addition, the LV expression of the ATP- and pyruvate-producing key enzyme in the last step of glycolysis, pyruvate kinase (*Pkm*), was markedly lower in the male DOXO-treated group and tended to decrease ($P = 0.09$) in the female DOXO-treated group compared with their sex-matched control groups (Fig. 8*F*). Interestingly, LV pyruvate levels were markedly higher in the female control group than in the male control group (Fig. 8*G*). In response to DOXO, the LV pyruvate levels were markedly reduced only in the female DOXO-treated group compared with the sex-matched control group (Fig. 8*G*). The lactate-producing lactate dehydrogenase (*Ldha*) was significantly repressed in the DOXO-treated females, and it showed a decreasing tendency ($P = 0.07$) in the DOXO-treated males compared with the sex-matched control groups (Fig. 8*H*). Similarly to pyruvate levels, LV lactate concentrations were significantly higher in control females than in control males (Fig. 7*I*). The LV lactate levels were markedly reduced only in the DOXO-treated females compared with the sex-matched control group (Fig. 8*I*). Notably, the lactate/pyruvate ratio was markedly lower in the DOXO-treated females compared with the DOXO-treated males, probably indicating better glucose utilization in aerobic glycolysis (Fig. 8*J*).

LV Carnitine Palmitoyltransferase-1α Was Repressed in Both Sexes, and Acyl-CoA Dehydrogenase Was Overexpressed in Females in Response to DOXO Treatment

In response to DOXO, serum triglyceride levels were increased only in males as compared with the sex-matched control group (Fig. 9*A*). The LV expression of carnitine palmitoyltransferase-1α (*Cpt1α*) was decreased in both DOXO-treated groups compared with the sex-matched control groups, suggesting disturbed transfer of the acyl group of a long-chain fatty acyl-CoA from coenzyme A to carnitine in the mitochondria (Fig. 9*B*). Notably, the LV expression of the first enzyme in the mitochondrial β-oxidation, i.e., acyl-CoA dehydrogenase (*Acadl*), showed an increasing tendency in the DOXO-treated males ($P = 0.06$) and was markedly elevated in the DOXO-treated females compared with the sex-matched control groups (Fig. 9*C*). There was no significant difference in the LV expression of the first enzyme in the peroxisomal β-oxidation of long-chain fatty acids, i.e., peroxisomal acyl-coenzyme A oxidase 1 (*Acox1*), among the groups (Fig. 9*D*). Serum total cholesterol, LDL, and HDL cholesterol levels were significantly elevated in the male DOXO-treated group compared with the sex-matched control group (Fig. 9, *E*–*G*). The LDL/HDL ratio did not differ significantly among the groups (Fig. 9*H*).

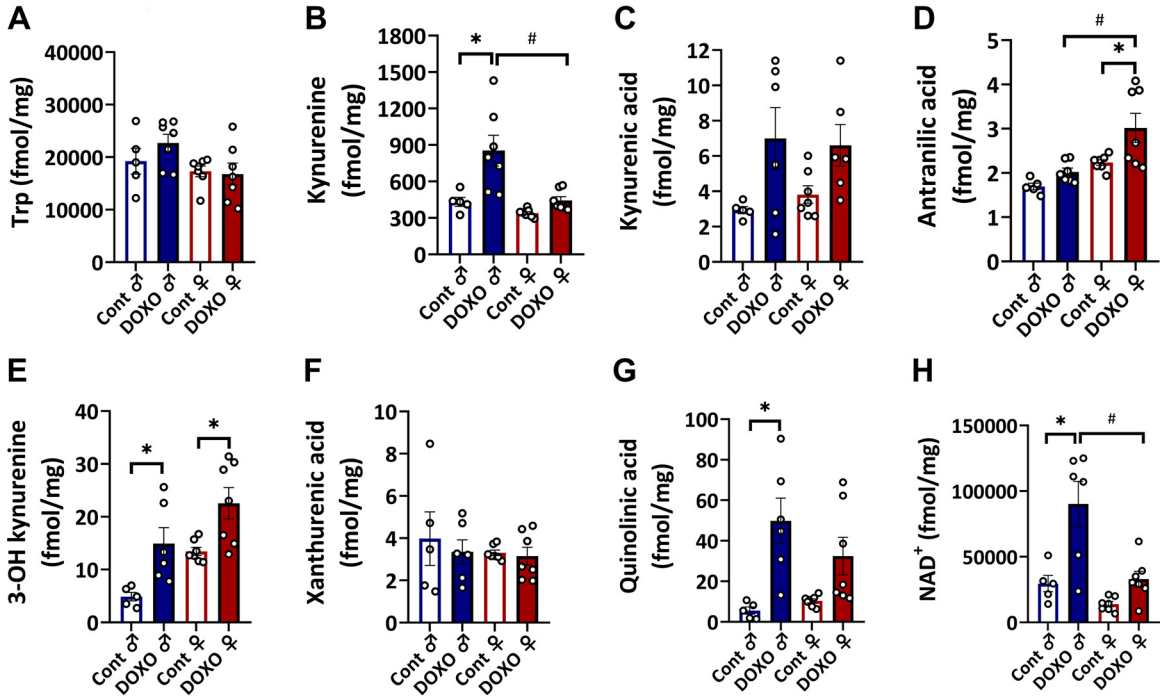

Figure 6. The effects of sex and DOXO on the left ventricular levels of tryptophan and its several metabolites in the kynurenine pathway. Tryptophan (Trp; *A*), kynurenine (*B*), kynurenic acid (*C*), anthranilic acid (*D*), 3-hydroxykynurenine (3-OH kynurenine, *E*), xanthurenic acid (*F*), quinolinic acid (*G*), and nicotinamide-adenine-dinucleotide (NAD^+, *H*). Values are presented as means ± SE, $*P < 0.05$ DOXO vs. control group, $\#P < 0.05$ females vs. males ($n = 5$–7 animals, one-way ANOVA, Holm–Sidak post hoc test). Cont, control; DOXO, doxorubicin.

DISCUSSION

In our present exploratory study, we have demonstrated that male animals developed DOXO-induced chronic cardiotoxicity at an accelerated rate, accompanied by more severe renal morphological and functional changes. Our descriptive results revealed sex-related changes in LV Trp metabolism accompanied by increased oxidative stress and

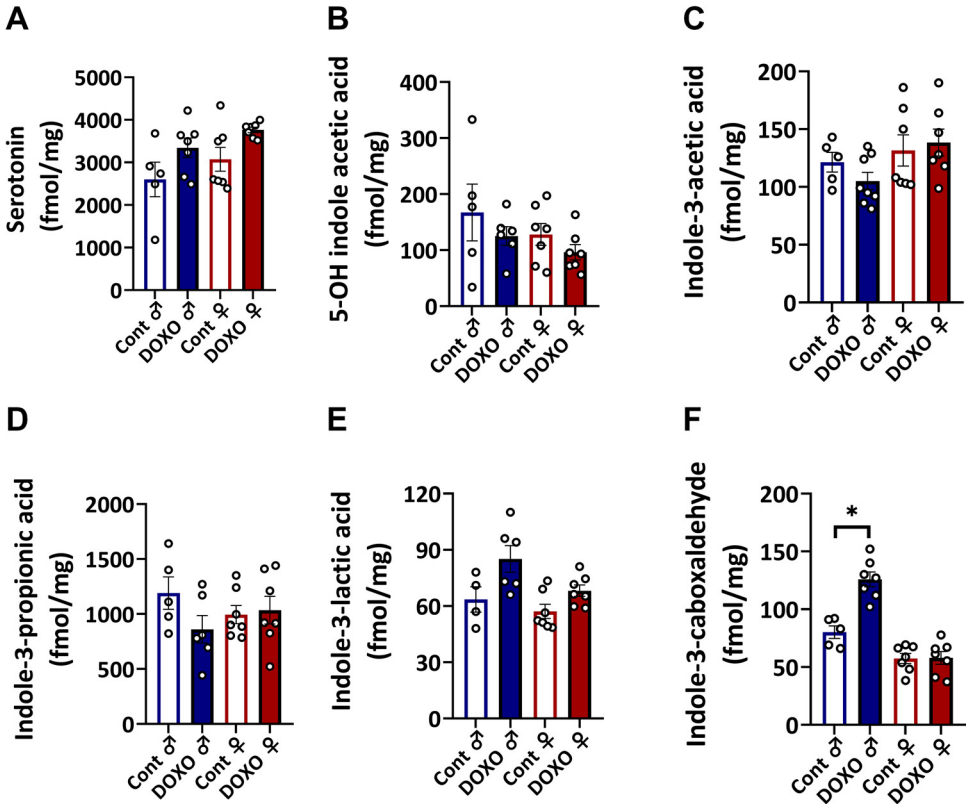

Figure 7. The effects of sex and DOXO on serotonin and several left ventricular metabolite levels in the indole pathway. Serotonin (*A*), 5-hydroxyindole acetic acid (*B*), indole-3-acetic acid (*C*), indole-3-propionic acid (*D*), indole-3-lactic acid (*E*), and indole-3-carboxaldehyde (*F*). Values are presented as means ± SE, $*P < 0.05$ DOXO vs. control group ($n = 5$–7 animals, one-way ANOVA, Holm–Sidak post hoc test). Cont, control; DOXO, doxorubicin.

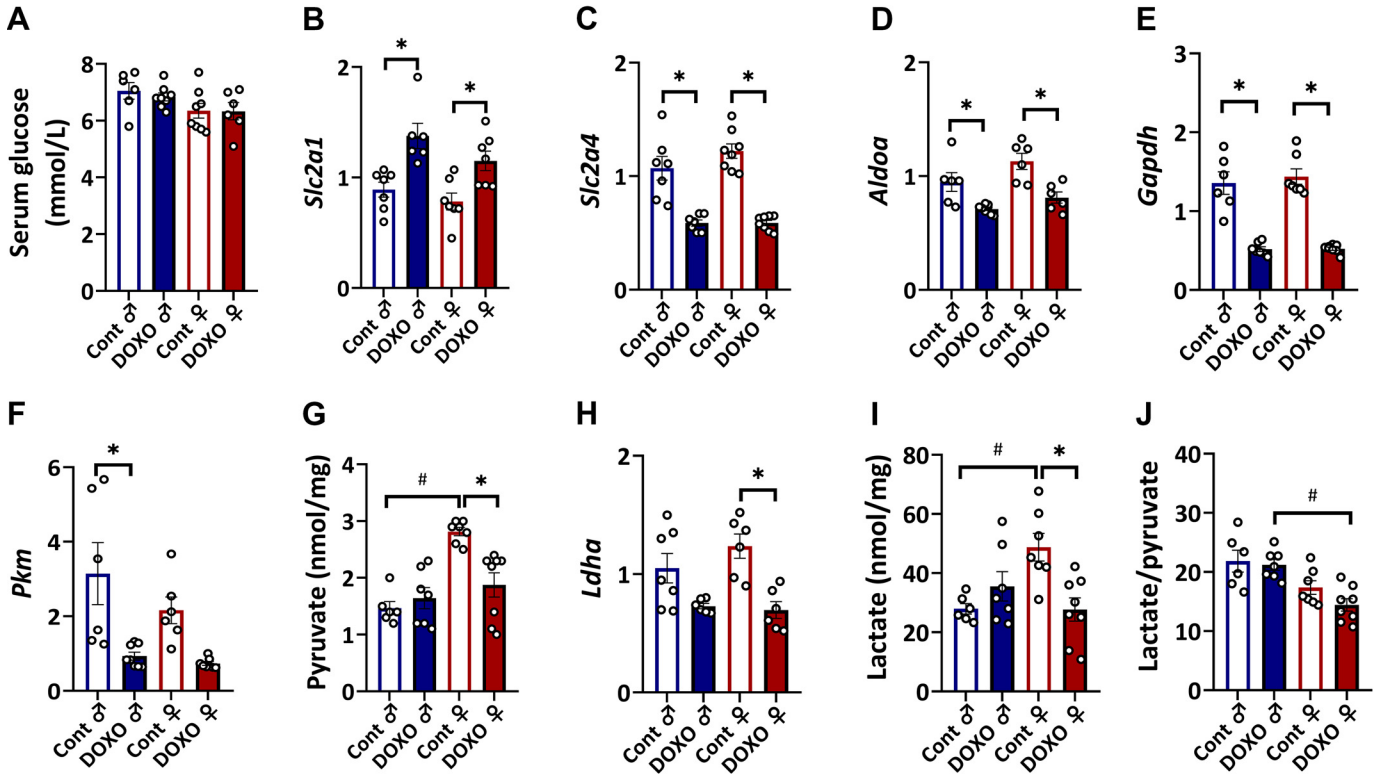

Figure 8. The effects of sex and DOXO on serum glucose levels, left ventricular gene expression, and metabolite concentrations related to glucose metabolism. Serum glucose (*A*), glucose transporter-1 (*Slc2a1*; *B*), glucose transporter 4 (*Slc2a4*; *C*), aldolase-A (*Aldoa*; *D*), glyceraldehyde-3-phosphate dehydrogenase (*Gapdh*; *E*), pyruvate kinase M1/M2 (*Pkm*; *F*), pyruvate (*G*), lactate dehydrogenase-A (*Ldha*; *H*), lactate (*I*), and lactate/pyruvate ratio (*J*). Values are presented as means ± SE, $*P < 0.05$ DOXO vs. control group, $\#P < 0.05$ females vs. males ($n = 6$–8 animals, one-way ANOVA, Holm–Sidak post hoc test). Cont, control; DOXO, doxorubicin.

inflammation, as well as altered glucose and fatty acid utilization, in the development of heart failure in DOXO-induced chronic cardiotoxicity. To the best of our knowledge, this study is the first to demonstrate sex-based differences in the LV levels of several Trp metabolites, including kynurenine, quinolinic acid, NAD^+, and indole-3-carboxaldehyde, in response to DOXO in a chronic cardiotoxicity model.

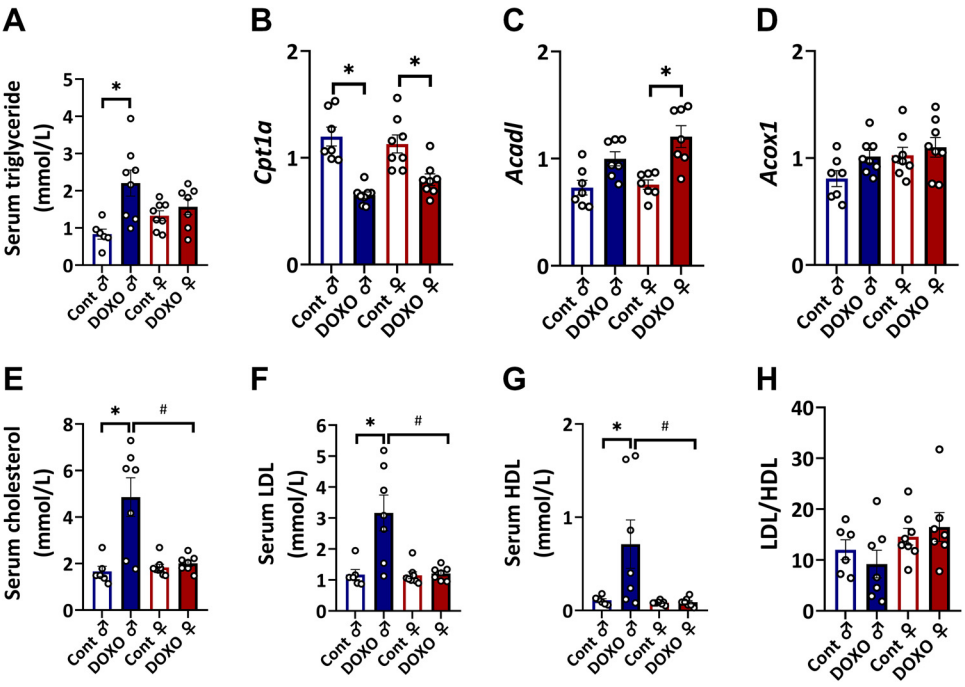

Figure 9. The effects of sex and DOXO on serum lipid levels and left ventricular gene expression related to lipid metabolism. Serum triglyceride (*A*), carnitine O-palmitoyltransferase-1α (*Cpt1α*; *B*), long-chain specific acyl-CoA dehydrogenase (*Acadl*; *C*), peroxisomal acyl-coenzyme A oxidase-1 (*Acox1*; *D*), serum cholesterol (*E*), serum LDL (*F*), serum HDL (*G*), and LDL/HDL (*H*) ratio. Values are presented as means ± SE, $*P < 0.05$ DOXO vs. control group, $\#P < 0.05$ females vs. males ($n = 6$–8 animals, one-way ANOVA, Holm–Sidak post hoc test). Cont, control; DOXO, doxorubicin.

We administered a cumulative DOXO dose of 6 mg/kg (equivalent to 420 mg/m^2 in patients), based on extrapolation of the clinical dose to rats, as detailed in the MATERIALS AND METHODS. A cumulative DOXO dose of > 350–400 mg/m^2 can cause DOXO-induced chronic cardiotoxicity with impaired EF (<50%), and a cumulative dose beyond 550 mg/m^2 increases the risk of the development of congestive heart failure in patients (42–44).

At *week 12*, there were no echocardiographic signs of morphological differences among the groups in our present study. However, only the DOXO-treated male group developed diastolic dysfunction (i.e., decreased e′ and increased E/e′). At the end point, both sexes exhibited echocardiographic and histological signs of DOXO-induced chronic cardiotoxicity, characterized by diastolic LV wall thinning, decreased relative wall thickness, and interstitial fibrosis, with concomitant diastolic dysfunction. Beyond LV structural alterations, such as LV hypertrophy and interstitial fibrosis, endothelial dysfunction may also contribute to diastolic dysfunction in patients, consistent with reduced LV *Nos3* expression in our present study (45, 46). During LV remodeling, surviving CMs may develop compensatory hypertrophy to maintain cardiac pump function, as evidenced by an increase in CM cross-sectional area in response to DOXO in both sexes in our present study (47). In response to DOXO, different patterns of hypertrophic remodeling may have distinct effects on ventricular geometry and function (48–50). Concentric LV hypertrophy resulting from increased CM width relative to length due to parallel addition of sarcomeres produces wall thickening and is often linked to diastolic dysfunction (51). In contrast, wall thinning, chamber dilation, and the dilated phenotype most often result from eccentric hypertrophy characterized by increased CM length relative to width due to assembly of sarcomeres in series (52). Since CM length-to-width ratios and other morphometric parameters were not assessed in the present study, we cannot determine whether the observed wall thinning reflects eccentric hypertrophic remodeling, CM loss, or a combination of these processes. In our present study, only the DOXO-treated male group exhibited a significant reduction in systolic function. In contrast, the DOXO-treated female group showed only a trend toward reduced EF at *week 19*. Moreover, LV dilatation (i.e., increased LVEDD, LVESD, LVEDV, and LVESV) and *Nppa* overexpression were more pronounced in the DOXO-treated male group, suggesting accelerated heart failure progression in males, consistent with previous studies (12, 53). Indeed, in adult patients, the majority of clinical studies reported more severe DOXO-induced chronic cardiotoxicity in men (5). Moreover, the total heart and LV weights were markedly reduced only in DOXO-treated males compared with sex-matched controls. Similar reductions in cardiac mass were reported in experimental models of DOXO-induced cardiotoxicity, driven by cardiac atrophy (50, 54). In contrast, CO was markedly higher in the male DOXO-treated group than in the male control group in our present study, likely due to the formula used for calculation (CO = SV × HR). In the DOXO-treated male group, both LVEDV and LVESV were significantly increased, resulting in a markedly higher SV than in the male control group. Probably as compensation for reduced EF, HR was slightly increased; however, this change was not significant ($P = 0.22$) in the DOXO-treated male group compared with the male control group. However, it should be acknowledged that volume measurements obtained with MRI or pressure-volume catheters may yield more accurate hemodynamic results than transthoracic echocardiography.

Although DOXO is acclaimed for its cardiotoxic effects in patients, it can cause chronic nephrotoxicity in both rodent models and humans, particularly with preexisting cardiovascular, kidney, and metabolic diseases (55–57). In our present study, despite mild renal fibrosis, there were no significant differences in blood pressure between DOXO-treated groups and their sex-matched controls, similar to previous studies using low DOXO doses to induce chronic cardiotoxicity (34, 58). However, only DOXO-treated males showed increased kidney weight and glomerular diameters, and elevated serum creatinine and urea levels, with a trend toward decreased creatinine clearance. Moreover, the LV concentration of the well-known uremic toxin and prooxidant indoxyl sulfate was markedly increased only in the DOXO-treated males (28). In contrast, DOXO-treated females exhibited proteinuria alone, suggesting less severe kidney injury, consistent with other studies on DOXO-induced nephrotoxicity models (59–61). In cardio-renal syndromes, the pathophysiology of heart failure and renal failure is closely interconnected by the reciprocal relationship between cardiac and renal injury (62). In our present study, the temporal relationship between renal injury and cardiac metabolic alterations cannot be determined because renal parameters were assessed at a single time point. Therefore, the impaired kidney function in the DOXO-treated males might contribute to or be a consequence of the accelerated chronic cardiotoxicity. Moreover, sex-based differences in the expression and activity of drug-metabolizing enzymes, such as cytochrome P450, may contribute to DOXO-induced cardiotoxicity and nephrotoxicity by mediating the metabolism of several biologically active endogenous compounds, including arachidonic acid and sexual steroids (60, 63–66). However, a more detailed characterization of sex-based differences in DOXO-induced nephrotoxicity was out of the scope of the present study, which focuses on LV changes in response to DOXO.

Increased oxidative stress and inflammation are well-known factors in the development of DOXO-induced cardiotoxicity (4, 6). Indeed, in our present study, the proinflammatory *Il6* was overexpressed in the left ventricle of the DOXO-treated male group. The LV GSH/GSSG ratio was markedly reduced in DOXO-treated males and tended to decrease in DOXO-treated females, indicating elevated oxidative stress. It is well known that increased oxidative stress can promote regulated cell death pathways, including apoptosis, pyroptosis, necroptosis, and ferroptosis (7). Recent evidence suggested that ferroptosis could play a crucial role in DOXO-induced cardiotoxicity (7). Interestingly, ferroptosis is triggered primarily by iron-dependent lipid peroxidation, which is driven by iron overload, glutathione (GSH) depletion, and the oxidation of polyunsaturated fatty acids in phospholipids (7).

The LV expression of *Nos3* was significantly reduced in both sexes in response to DOXO, suggesting a decrease in LV nitric oxide (NO) synthesis. It has been reported that reduced

eNOS expression might contribute to uncoupling, a process in which eNOS produces superoxide rather than NO, further exacerbating oxidative stress, inflammation, and endothelial dysfunction (67). Beyond endothelial cells, *Nos3* is also expressed in CMs, where its depletion may contribute to cardiac remodeling, including hypertrophy and fibrosis (68). Moreover, in our present study, the L-arginine metabolites ADMA and SDMA levels were markedly increased in the left ventricles of males in response to DOXO, consistent with previous human and cell-based studies (69, 70). It has been reported that ADMA directly inhibits eNOS. SDMA can reduce L-arginine availability by competing with it for cellular transport, thereby indirectly causing eNOS uncoupling and diminished NO production, leading to elevated nitro-oxidative stress, inflammation, hypertrophy, and fibrosis (69, 71–73). Moreover, elevated plasma levels of ADMA in patients with heart failure are associated with increased oxidative stress and impaired glomerular filtration (74). Elevated plasma SDMA levels are associated with the progression of chronic kidney disease by increasing the expression of proinflammatory cytokines, including IL-6 and TNF-α (71). In our present study, sex-based differences in ADMA and SDMA levels, the GSH/GSSG ratio, and *Il6* overexpression may contribute to the accelerated DOXO-induced chronic cardiotoxicity in males. Notably, the reduction in *Nos3* expression observed in DOXO-treated females, despite the lack of significant changes in LV ADMA and SDMA levels, indicates that *Nos3* expression and regulation involve further factors and mechanisms. In our present study, LV *Nos3* expression was measured at the transcript level rather than the protein level, which limits the interpretation of the results. Beyond ADMA and SDMA levels, the expression and activity of NOS3 protein could also be modified by a complex network, including changes in microRNA levels, hormonal and metabolic status (e.g., estrogen, hyperglycemia, and hyperinsulinemia), the availability of its cofactors (e.g., calcium ions, L-arginine, and tetrahydrobiopterin), protein-protein interactions (e.g., heat shock proteins), elevated nitro-oxidative stress, and posttranscriptional changes, such as phosphorylation, *S*-glutathionylation, etc. (75–78). However, the investigation of these factors was out of the scope of our present study.

Here, we measured key tryptophan (Trp) metabolites, particularly those involved in the kynurenine pathway, in the left ventricle after DOXO treatment. Trp metabolism can be modulated by inflammation, thereby exacerbating cardiovascular diseases (17). A central metabolite of the kynurenine pathway is kynurenine, a pluripotent intermediate in the biosynthesis of further metabolites that participate in inflammation and metabolism (17). In our present study, LV kynurenine levels were increased in DOXO-treated males, consistent with a previous study on DOXO-induced cardiotoxicity in male mice (79). Moreover, elevated plasma levels of kynurenine have been linked to heart failure and cardiac remodeling in patients (23, 24). Under chronic inflammatory conditions, such as chronic kidney disease or DOXO-induced cardiac injury, an imbalance may occur between the proinflammatory and anti-inflammatory downstream products of the kynurenine pathway (80, 81). Kynurenic acid is a promising therapeutic agent for DOXO-induced cardiotoxicity, as it has been reported to enhance mitochondrial function, reduce oxidative stress, and inhibit the ATP synthase inhibitory subunit 1 (82). However, in our present study, kynurenic acid levels were not significantly changed by DOXO in either sex ($P = 0.12$ in males and $P = 0.22$ in females).

In our present study, LV anthranilic acid levels were markedly increased only in the DOXO-treated females. In a study on aortic root tissues, anthranilic acid treatment reduced oxidative stress and inhibited the release of proinflammatory cytokines (IL-1β, IL-6, and TNF-α) from macrophages and endothelial cells (83). In experimental models, a synthetic analog of anthranilic acid, tranilast, alleviated diastolic dysfunction, cardiac fibrosis, and hypertrophy, and reduced albuminuria and plasma creatinine levels in diabetic rats by blocking transforming growth factor-β (18). Furthermore, a study examining DOXO-induced myocardial damage found that tranilast reduced cardiac apoptosis, hypertrophy, fibrosis, and functional and ECG changes (47). In our present study, the redirection of Trp away from degradation via the kynurenine pathway may explain the increased anthranilic acid levels in DOXO-treated females, suggesting a compensatory mechanism to alleviate DOXO-induced chronic cardiotoxicity.

In our present study, we observed a significant increase in 3-hydroxykynurenine in both sexes of DOXO-treated animals. Inflammation can increase the production of 3-hydroxykynurenine, a controversial metabolite with both antioxidant and prooxidant properties (19, 20). In clinical studies, elevated plasma levels of 3-hydroxykynurenine have been associated with inflammation and oxidative stress in heart failure and chronic kidney disease (24, 84). The elevation of 3-hydroxykynurenine in both sexes, alongside a male-specific increase in quinolinic acid, might be explained by sex-dependent regulation of the enzyme 3-hydroxyanthranilate-3,4-dioxygenase responsible for converting 3-hydroxykynurenine to the downstream metabolite quinolinic acid, rather than simply the initial production of 3-hydroxykynurenine (85).

Under physiological conditions, quinolinic acid serves as a precursor in the synthesis of NAD^+, a critical cofactor for cellular functions. However, in excess, quinolinic acid can exert inflammatory effects via IL-1 and IL-6, disrupting the oxidant/antioxidant balance. It forms stable iron complexes, thereby increasing lipid peroxidation and hydroxyl radical generation, enhancing peroxynitrite formation, and altering the reduced glutathione/oxidized glutathione ratio (25, 86). Notably, quinolinic acid can enhance NAD^+ production, which is essential for cardiac cells to meet their increased energy demands in heart failure (15). Indeed, in our present study, LV quinolinic acid and NAD^+ levels were significantly increased in the DOXO-treated males and showed only a tendency to increase in the DOXO-treated females. Consequently, we hypothesized that more pronounced oxidative stress and inflammation might activate the kynurenine pathway to a greater extent, resulting in higher levels of the end product, NAD^+, in DOXO-treated males than in females. These metabolic changes might represent an adaptive response to the accelerated heart failure observed in the male DOXO-treated group. However, it should be noted that NAD^+ levels alone, without the NAD^+/NADH ratio, provide limited information about cellular redox state and metabolic health. Our next step was to investigate the metabolic utilization of NAD^+ in glycolysis.

The adult heart generates ATP primarily through mitochondrial oxidative phosphorylation (~95%) and cytoplasmic glycolysis (~5%) (87). CMs responsible for pump function constitute 70%–85% of the total volume of the adult mammalian heart but only represent ~25%–35% of the total number of cells (88). Although non-CMs, such as vascular smooth muscle cells, endothelial cells, and fibroblasts, occupy a smaller volume fraction, they are essential for normal heart structure and function, providing the extracellular matrix, intercellular communication, and blood supply needed for efficient CM contraction (88). Both CMs and non-CMs respond to stress, and maladaptive changes in non-CMs, such as fibrosis or reduced capillary density, participate in the pathogenesis of heart failure (88). Under physiological conditions, endothelial cells, activated fibroblasts, and, in particular, CMs prefer mitochondrial β-oxidation of free fatty acids for ATP production (87, 89). β-Oxidation produces 129 ATP from palmitic acid. Under physiological circumstances, glucose is taken up mainly via the insulin-dependent glucose transporter GLUT4 and, to a lesser extent, via the insulin-independent GLUT1 to the adult heart (90). Glucose contributes to ATP production by 25%–30% via both mitochondrial pyruvate oxidation, which yields 36–38 ATP molecules, and anaerobic glycolysis, which produces only 2 ATP molecules and lactate (87, 90). Although glucose is not the predominant fuel for the healthy adult heart, the heart switches its substrate preference from free fatty acids to glucose under various circumstances, including hypertrophy and progressive heart failure (90). Glycolysis requires NAD^+ molecules in the GAPDH-catalyzed step (87). In heart failure, mitochondrial oxidative capacity declines, leading to reduced ATP production via β-oxidation of free fatty acids or pyruvate oxidation from glucose (87). In heart failure, the heart attempts to compensate for the imbalance between energy demand and supply by increasing insulin-independent glucose uptake and by shifting metabolism toward glycolysis. Indeed, in our present study, the insulin-independent glucose transporter *Slc2a1* was overexpressed, whereas the insulin-dependent glucose transporter *Slc2a4* was repressed in both DOXO-treated groups, consistent with previous preclinical and clinical findings (12, 91). However, in our hands, the aerobic glycolytic enzymes (i.e., *Aldoa* and *Gapdh* in both sexes and *Pkm* in males) and the anaerobic *Ldh* (in females) were significantly repressed in the DOXO-treated animals, indicating a disturbance in glucose utilization by aerobic or anaerobic glycolysis, contrary to our expectations and literature data (91). However, in pressure-overload-induced heart failure, the decline in glycolysis and glucose oxidation was shown to be an early metabolic change in the development of cardiac hypertrophy with diastolic dysfunction (92). Notably, the lactate/pyruvate ratio was significantly reduced in DOXO-treated females compared with DOXO-treated males, suggesting better glucose utilization in females. We speculate that the significantly higher NAD^+ levels in DOXO-treated males and the slightly higher levels in females may result from repression of *Gapdh*, as less NAD^+ is consumed in this reaction.

In our present study, serum triglyceride and cholesterol levels were increased in DOXO-treated males, as reported in our previous study and by others (34, 93). Hyperlipidemia may be attributed to DOXO-induced peroxisome proliferator-activated receptor γ inhibition, leading to decreased lipid clearance, lipotoxicity, and inflammation (93). In our present study, LV repression of mitochondrial carnitine palmitoyltransferase 1α (*Cpt1α*) in response to DOXO may indicate a disturbance in the transport of acyl groups from the cytoplasm to mitochondrial β-oxidation enzymes. Interestingly, the first enzyme in mitochondrial β-oxidation (i.e., *Acadl*) was overexpressed in DOXO-treated females, suggesting greater compensation and utilization of free fatty acids, which might explain their less severe heart failure than in DOXO-treated males. Indeed, Zhang et al. (92) demonstrated in pressure-overload-induced heart failure that a decline in fatty acid oxidation was associated with a transition from diastolic dysfunction to systolic dysfunction.

Conclusions

In our rat model, DOXO treatment induced LV wall thinning and cardiac fibrosis with diastolic dysfunction, repression of endothelial nitric oxide synthase at the transcript level, and disturbed glucose (i.e., overexpression of *Slc2a1* and repression of *Aldoa* and *Gapdh*) and fatty acid (i.e., repression of *Cpt1α*) metabolism, as well as mild renal fibrosis in both sexes. DOXO-treated males developed chronic cardiotoxicity at an accelerated rate, characterized by left ventricular dilation and decreased ejection fraction, and renal dysfunction with increased glomerular diameters, serum urea, and creatinine levels. Moreover, DOXO-treated males exhibited increased serum triglyceride and cholesterol concentrations. They also displayed more pronounced changes in LV gene expression and metabolite levels associated with oxidative stress (e.g., increased ADMA and SDMA levels, reduced GSH/GSSG ratio, and *Nos3* repression) and inflammation (e.g., *Il6* overexpression). Importantly, LV concentrations of several Trp metabolites associated with oxidative stress and inflammation (e.g., kynurenine and quinolinic acid), energy metabolism (NAD^+), and fibrosis (e.g., indoxyl sulfate) were higher in DOXO-treated males. Our results align with the existing literature, suggesting that males may be more susceptible to DOXO-induced cardiac damage. Our present findings suggest that sex-based differences in LV Trp metabolism, oxidative stress, inflammation, and energy metabolism in response to DOXO are associated with the accelerated development of heart failure with systolic dysfunction in males (Fig. 10). However, further studies are needed to determine whether these sex-based differences, particularly in the LV Trp metabolite concentrations, are causes or consequences of the accelerated disease progression in the DOXO-treated males. DOXO-treated females exhibited less severe renal dysfunction and higher LV mitochondrial acyl-CoA dehydrogenase expression, suggesting improved fatty acid utilization, which might explain their better systolic function.

Limitations

The potential protective role of female hormones, particularly estrogen, in DOXO-induced cardiotoxicity was not thoroughly explored in this study (e.g., by ovariectomy or administration of estrogen to males). Although previous studies suggest that estrogen may offer cardioprotective effects, our focus was more on the descriptive characterization of

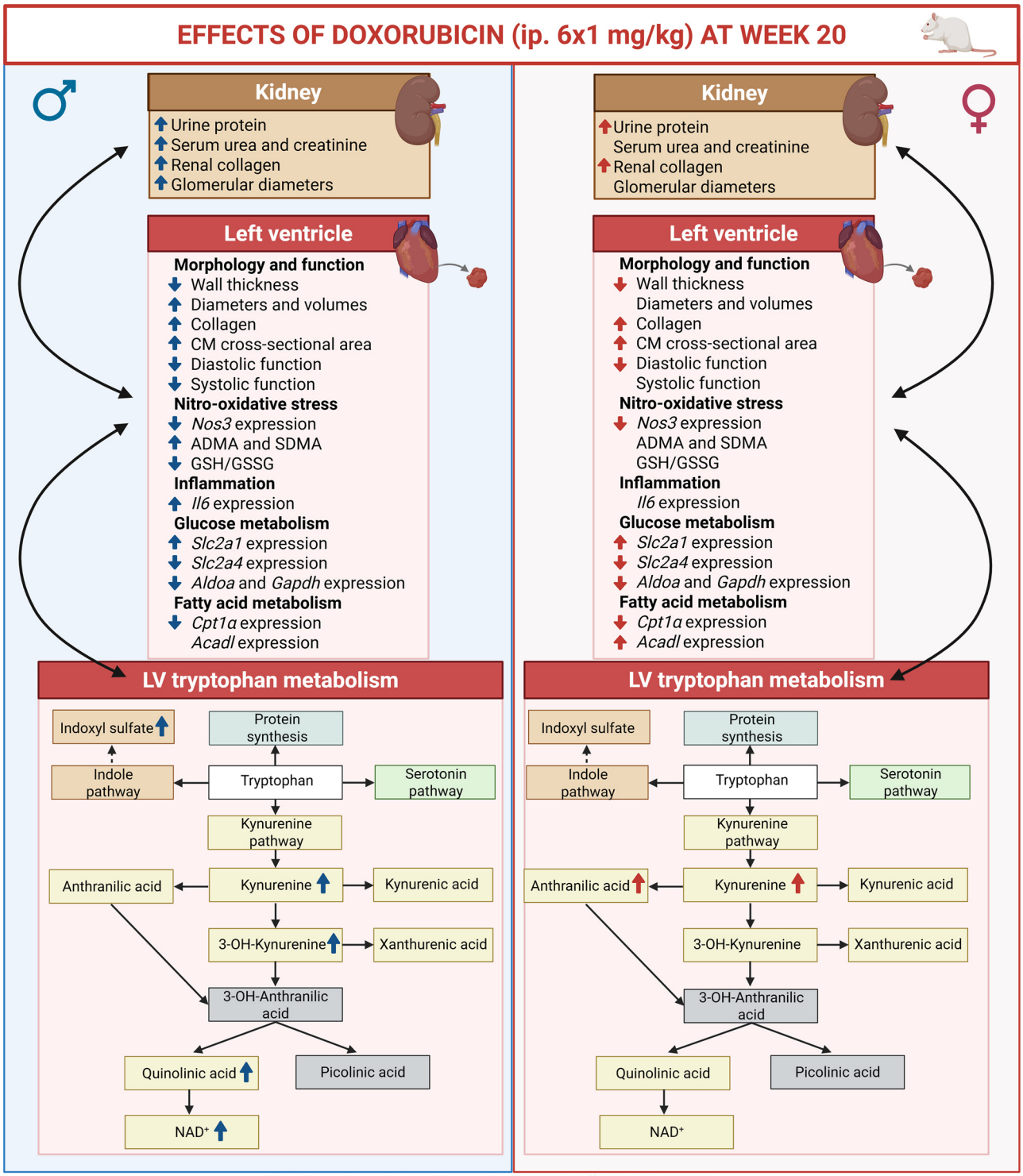

https://app.biorender.com/illustrations/69e89d6bff0b682ddb9d2075

Figure 10. Sex-based differences and putative organ crosstalk in DOXO-induced chronic cardiotoxicity and nephrotoxicity. *Acadl*, long-chain specific acyl-CoA dehydrogenase; ADMA, asymetric dimethyl arginine; *Aldoa*, aldolase-A; CM, cardiomyocyte; *Cpt1α*, carnitine O-palmitoyltransferase-1α; *Gapdh*, glyceraldehyde-3-phosphate dehydrogenase; GSH/GSSG, reduced to oxidized glutathione ratio; *Il6*, interleukin-6; LV, left ventricular; *Nos3*, endothelial nitric oxide synthase; SDMA, syMetric dimethyl arginine; *Slc2a1*, glucose transporter-1; *Slc2a4*, glucose transporter 4. Figure created with a licensed version of BioRender.com. DOXO, doxorubicin.

sex-based differences in response to DOXO. A detailed analysis of hormonal levels could provide further insight into the sex-based differences in the development of DOXO-induced chronic cardiotoxicity. The applicability of our findings is limited by the absence of aging and comorbidities, such as cancer or other relevant cardiovascular risk factors. Moreover, our present findings are limited to the follow-up time points (i.e., 12 and 19 wk for echocardiography,

and 20 wk for histology and biochemical measurements in tissue samples) and do not rule out the possibility that females may develop DOXO-induced chronic cardiotoxicity and renal dysfunction of similar severity at a later time point. Importantly, our exploratory study is mainly descriptive and correlative; therefore, the observed metabolic alterations, particularly changes in Trp metabolite levels, cannot be interpreted as direct causes or consequences of DOXO-induced chronic cardiotoxicity. Therefore, a more detailed exploration of the molecular mechanisms, including analysis of gene expression at the transcript and protein levels, as well as post-transcriptional modifications of proteins, underlying the observed sex-based differences in Trp metabolism, would be essential to elucidate the pathways and interactions between different cell types involved in DOXO-induced chronic cardiotoxicity in future studies.

DATA AVAILABILITY

The datasets used and/or analyzed during the current study are available from the corresponding author upon reasonable request.

SUPPLEMENTAL MATERIAL

Supplemental Figs. S1–S4: https://doi.org/10.17605/OSF.IO/EVJSD.

ACKNOWLEDGMENTS

We thank Krisztián Daru for the excellent histological slide preparation and staining. We thank Dr. Bálint Cserni for creating the program for the picrosirius red and fast green image analysis. Graphical abstract and Fig. 10 created with a licensed version of BioRender.com.

GRANTS

The present work was supported by the projects of the National Research, Development, and Innovation Office, Hungary (Grant Nos. NKFIH FK129094, FK138223, and GINOP-2.3.2-15-2016-00040, and 2024-1.2.11-TÉT-IPARI-TR-2025-00038) and the University of Szeged Grant Nos. SZAOK-KKA-SZGYA-5S170-A202, and -5S422 A202. M. Sárközy and A. Sejben were supported by the János Bolyai Research Fellowship of the Hungarian Academy of Sciences Grant No. BO/00532/23/5 and BO/00340/25.

DISCLOSURES

Single-Cell Technologies Ltd., Szeged, Hungary, developed the Biology Image Analysis Software (BIAS). Prof. Dr. P. Horváth is the CEO, A. Kriston and F. Kovács are software engineers at Single-Cell Technologies Ltd. None of the other authors has any conflicts of interest, financial or otherwise, to disclose.

AUTHOR CONTRIBUTIONS

K.K., Z.K., and M.S. conceived and designed research; K.K., Z.G., R.L., D.V., A. Siska, A. Sejben, M. Kohistani, M. Kis, R.S., Z.A.G., A.K., F.K., P.H., P.B., and M.S. performed experiments; K.K., Z.G., D.V., A. Siska, A. Sejben, and M. Kohistani analyzed data; K.K., Z.G., D.V., A. Sejben, P.B., I.F., P.M., G.C., Z.K., and M.S. interpreted results of experiments; K.K. and Z.G. prepared figures; K.K., Z.G., and M.S. drafted manuscript; K.K., A. Sejben, P.H., P.B., I.F., P.M., G.C., Z.K., and M.S. edited and revised manuscript; K.K., Z.G., R.L., D.V., A. Siska, A. Sejben, M. Kohistani, M. Kis, R.S., Z.A.G., A.K., F.K., P.H., P.B., I.F., P.M., G.C., Z.K., and M.S. approved final version of manuscript.

REFERENCES

1. Global, regional, and national age-sex-specific mortality for 282 causes of death in 195 countries and territories, 1980-2017: a systematic analysis for the Global Burden of Disease Study 2017. *Lancet* 392: 1736–1788, 2018 [Erratum in *Lancet* 393: e44, 2019; Erratum in *Lancet* 392: 2170, 2018]. doi:10.1016/S0140-6736(18)32203-7.
2. **Miller KD**, **Nogueira L**, **Mariotto AB**, **Rowland JH**, **Yabroff KR**, **Alfano CM**, **Jemal A**, **Kramer JL**, **Siegel RL.** Cancer treatment and survivorship statistics, 2019. *CA Cancer J Clin* 69: 363–385, 2019. doi:10.3322/caac.21565.
3. **Lenneman CG**, **Sawyer DB.** Cardio-oncology: an update on cardiotoxicity of cancer-related treatment. *Circ Res* 118: 1008–1020, 2016. doi:10.1161/CIRCRESAHA.115.303633.
4. **Linders AN**, **Dias IB**, **López Fernández T**, **Tocchetti CG**, **Bomer N**, **van der Meer P.** A review of the pathophysiological mechanisms of doxorubicin-induced cardiotoxicity and aging. *NPJ Aging* 10: 9, 2024. doi:10.1038/s41514-024-00135-7.
5. **Meiners B**, **Shenoy C**, **Zordoky BN.** Clinical and preclinical evidence of sex-related differences in anthracycline-induced cardiotoxicity. *Biol Sex Differ* 9: 38, 2018. doi:10.1186/s13293-018-0198-2.
6. **Sheibani M**, **Azizi Y**, **Shayan M**, **Nezamoleslami S**, **Eslami F**, **Farjoo MH**, **Dehpour AR.** Doxorubicin-induced cardiotoxicity: an overview on pre-clinical therapeutic approaches. *Cardiovasc Toxicol* 22: 292–310, 2022. doi:10.1007/s12012-022-09721-1.
7. **Wu L**, **Zhang Y**, **Wang G**, **Ren J.** Molecular mechanisms and therapeutic targeting of ferroptosis in doxorubicin-induced cardiotoxicity. *JACC Basic Transl Sci* 9: 811–826, 2024. doi:10.1016/j.jacbts.2023.10.009.
8. **Wang A J**, **Zhang J**, **Xiao M**, **Wang S**, **Wang B J**, **Guo Y**, **Tang Y**, **Gu J.** Molecular mechanisms of doxorubicin-induced cardiotoxicity: novel roles of sirtuin 1-mediated signaling pathways. *Cell Mol Life Sci* 78: 3105–3125, 2021. doi:10.1007/s00018-020-03729-y.
9. **Sangweni NF**, **van Vuuren D**, **Mabasa L**, **Gabuza K**, **Huisamen B**, **Naidoo S**, **Barry R**, **Johnson R.** Prevention of anthracycline-induced cardiotoxicity: the good and bad of current and alternative therapies. *Front Cardiovasc Med* 9: 907266, 2022. doi:10.3389/fcvm.2022.907266.
10. **Wang Y**, **Wang Y**, **Han X**, **Sun J**, **Li C**, **Adhikari BK**, **Zhang J**, **Miao X**, **Chen Z.** Cardio-oncology: a myriad of relationships between cardiovascular disease and cancer. *Front Cardiovasc Med* 9: 727487, 2022. doi:10.3389/fcvm.2022.727487.
11. **Su Q**, **Fu M**, **Xiao W**, **Zhao H**, **Yu Y**, **Feng J**, **Liu Y**, **Wan Y**, **Yu Y**, **Zhang C.** Sex differences in doxorubicin-induced cardiotoxicity: insights from transcriptome analysis. *Adv Ther (Weinh)* 7: 2400036, 2024. doi:10.1002/adtp.202400036.
12. **Moulin M**, **Piquereau J**, **Mateo P**, **Fortin D**, **Rucker-Martin C**, **Gressette M**, **Lefebvre F**, **Gresikova M**, **Solgadi A**, **Veksler V**, **Garnier A**, **Ventura-Clapier R.** Sexual dimorphism of doxorubicin-mediated cardiotoxicity: potential role of energy metabolism remodeling. *Circ Heart Fail* 8: 98–108, 2015. doi:10.1161/CIRCHEARTFAILURE.114.001180.
13. **Walker MA**, **Tian R.** NAD metabolism and heart failure: mechanisms and therapeutic potentials. *J Mol Cell Cardiol* 195: 45–54, 2024. doi:10.1016/j.yjmcc.2024.07.008.
14. **Chandel NS.** NADPH-the forgotten reducing equivalent. *Cold Spring Harb Perspect Biol* 13: a040550, 2021. doi:10.1101/cshperspect.a040550.
15. **Wu Y**, **Pei Z**, **Qu P.** NAD^+- a hub of energy metabolism in heart failure. *Int J Med Sci* 21: 369–375, 2024. doi:10.7150/ijms.89370.
16. **Yang Y**, **Liu X**, **Liu X**, **Xie C**, **Shi J.** The role of the kynurenine pathway in cardiovascular disease. *Front Cardiovasc Med* 11: 1406856, 2024. doi:10.3389/fcvm.2024.1406856.
17. **Grishanova AY**, **Perepechaeva ML.** Kynurenic acid/AhR signaling at the junction of inflammation and cardiovascular diseases. *Int J Mol Sci* 25: 6933, 2024. doi:10.3390/ijms25136933.

18. **Darakhshan S**, **Pour AB.** Tranilast: a review of its therapeutic applications. *Pharmacol Res* 91: 15–28, 2015. doi:10.1016/j.phrs.2014.10.009.
19. **Hayes AJ**, **Zheng X**, **O'Kelly J**, **Neyton LPA**, **Bochkina NA**, **Uings I**, **Liddle J**, **Baillie JK**, **Just G**, **Binnie M**, **Homer NZM**, **Murray TBJ**, **Baily J**, **McGuire K**, **Skouras C**, **Garden OJ**, **Webster SP**, **Iredale JP**, **Howie SEM**, **Mole DJ.** Kynurenine monooxygenase regulates inflammation during critical illness and recovery in experimental acute pancreatitis. *Cell Rep* 42: 112763, 2023. doi:10.1016/j.celrep.2023.112763.
20. **Baran H**, **Staniek K**, **Bertignol-Spörr M**, **Attam M**, **Kronsteiner C**, **Kepplinger B.** Effects of various kynurenine metabolites on respiratory parameters of rat brain, liver and heart mitochondria. *Int J Tryptophan Res* 9: 17–29, 2016. doi:10.4137/IJTR.S37973.
21. **Castro-Portuguez R**, **Sutphin GL.** Kynurenine pathway, NAD^+ synthesis, and mitochondrial function: targeting tryptophan metabolism to promote longevity and healthspan. *Exp Gerontol* 132: 110841, 2020. doi:10.1016/j.exger.2020.110841.
22. **Wirthgen E**, **Hoeflich A**, **Rebl A**, **Günther J.** Kynurenic acid: the Janus-faced role of an immunomodulatory tryptophan metabolite and its link to pathological conditions. *Front Immunol* 8: 1957, 2018. doi:10.3389/fimmu.2017.01957.
23. **Lewkowicz J**, **Tankiewicz-Kwedlo A**, **Pawlak D**, **Kiluk M**, **Łagoda K**, **Kowalska I.** Kynurenines in heart failure with preserved ejection fraction: an influence of type 2 diabetes. *Pol Arch Intern Med* 134: 16837, 2024. doi:10.20452/pamw.16837.
24. **Lund A**, **Nordrehaug JE**, **Slettom G**, **Solvang S-EH**, **Pedersen EKR**, **Midttun Ø**, **Ulvik A**, **Ueland PM**, **Nygård O**, **Giil LM.** Plasma kynurenines and prognosis in patients with heart failure. *PLoS One* 15: e0227365, 2020 [Erratum in *PLoS One* 15: e0230056, 2020]. doi:10.1371/journal.pone.0230056.
25. **Wang Q**, **Liu D**, **Song P**, **Zou MH.** Tryptophan-kynurenine pathway is dysregulated in inflammation, and immune activation. *Front Biosci (Landmark Ed)* 20: 1116–1143, 2015. doi:10.2741/4363.
26. **Yan J**, **Chen D**, **Ye Z**, **Zhu X**, **Li X**, **Jiao H**, **Duan M**, **Zhang C**, **Cheng J**, **Xu L**, **Li H**, **Yan D.** Molecular mechanisms and therapeutic significance of tryptophan metabolism and signaling in cancer. *Mol Cancer* 23: 241, 2024. doi:10.1186/s12943-024-02164-y.
27. **Rieder M**, **Gauchel N**, **Bode C**, **Duerschmied D.** Serotonin: a platelet hormone modulating cardiovascular disease. *J Thromb Thrombolysis* 52: 42–47, 2021. doi:10.1007/s11239-020-02331-0.
28. **Gao H**, **Liu S.** Role of uremic toxin indoxyl sulfate in the progression of cardiovascular disease. *Life Sci* 185: 23–29, 2017. doi:10.1016/j.lfs.2017.07.027.
29. **Wang YC**, **Koay YC**, **Pan C**, **Zhou Z**, **Tang W**, **Wilcox J**, **Li XS**, **Zagouras A**, **Marques F**, **Allayee H**, **Rey FE**, **Kaye DM**, **O'Sullivan JF**, **Hazen SL**, **Cao Y**, **Lusis AJ.** Indole-3-propionic acid protects against heart failure with preserved ejection fraction. *Circ Res* 134: 371–389, 2024. doi:10.1161/CIRCRESAHA.123.322381.
30. **Podyacheva EY**, **Kushnareva EA**, **Karpov AA**, **Toropova YG.** Analysis of models of doxorubicin-induced cardiomyopathy in rats and mice. A modern view from the perspective of the pathophysiologist and the clinician. *Front Pharmacol* 12: 670479, 2021. doi:10.3389/fphar.2021.670479.
31. **Feijen EAM**, **Leisenring WM**, **Stratton KL**, **Ness KK**, **van der Pal HJH**, **van Dalen EC**, **Armstrong GT**, **Aune GJ**, **Green DM**, **Hudson MM**, **Loonen J**, **Oeffinger KC**, **Robison LL**, **Yasui Y**, **Kremer LCM**, **Chow EJ.** Derivation of anthracycline and anthraquinone equivalence ratios to doxorubicin for late-onset cardiotoxicity. *JAMA Oncol* 5: 864–871, 2019. doi:10.1001/jamaoncol.2018.6634.
32. **Escher SE**, **Batke M**, **Hoffmann-Doerr S**, **Messinger H**, **Mangelsdorf I.** Interspecies extrapolation based on the RepDose database–a probabilistic approach. *Toxicol Lett* 218: 159–165, 2013. doi:10.1016/j.toxlet.2013.01.027.
33. **Sharma V**, **McNeill JH.** To scale or not to scale: the principles of dose extrapolation. *Br J Pharmacol* 157: 907–921, 2009. doi:10.1111/j.1476-5381.2009.00267.x.
34. **Freiwan M**, **Kovács MG**, **Kovács ZZA**, **Szűcs G**, **Dinh H**, **Losonczi R**, **Siska A**, **Kriston A**, **Kovács F**, **Horváth P**, **Földesi I**, **Cserni G**, **Dux L**, **Csont T**, **Sárközy M.** Investigation of the antiremodeling effects of losartan, mirabegron and their combination on the development of doxorubicin-induced chronic cardiotoxicity in a rat model. *Int J Mol Sci* 23: 2201, 2022. doi:10.3390/ijms23042201.
35. **Sárközy M**, **Watzinger S**, **Kovács ZZA**, **Acar E**, **Márványkövi F**, **Szűcs G**, **Lauber GY**, **Galla Z**, **Siska A**, **Földesi I**, **Fintha A**, **Kriston A**, **Kovács F**, **Horváth P**, **Kővári B**, **Cserni G**, **Krenács T**, **Szabó PL**, **Szabó GT**, **Monostori P**, **Zins K**, **Abraham D**, **Csont T**, **Pokreisz P**, **Podesser BK**, **Kiss A.** Neuregulin-1β improves uremic cardiomyopathy and renal dysfunction in rats. *JACC Basic Transl Sci* 8: 1160–1176, 2023. doi:10.1016/j.jacbts.2023.03.003.
36. **Sárközy M**, **Márványkövi FM**, **Szűcs G**, **Kovács ZZA**, **Szabó MR**, **Gáspár R**, **Siska A**, **Kővári B**, **Cserni G**, **Földesi I**, **Csont T.** Ischemic preconditioning protects the heart against ischemia-reperfusion injury in chronic kidney disease in both males and females. *Biol Sex Differ* 12: 49, 2021. doi:10.1186/s13293-021-00392-1.
37. **Kovács ZZA**, **Szűcs G**, **Freiwan M**, **Kovács MG**, **Márványkövi FM**, **Dinh H**, **Siska A**, **Farkas K**, **Kovács F**, **Kriston A**, **Horváth P**, **Kővári B**, **Cserni BG**, **Cserni G**, **Földesi I**, **Csont T**, **Sárközy M.** Comparison of the antiremodeling effects of losartan and mirabegron in a rat model of uremic cardiomyopathy. *Sci Rep* 11: 17495, 2021. doi:10.1038/s41598-021-96815-5.
38. **Kovács MG**, **Kovács ZZA**, **Varga Z**, **Szűcs G**, **Freiwan M**, **Farkas K**, **Kővári B**, **Cserni G**, **Kriston A**, **Kovács F**, **Horváth P**, **Földesi I**, **Csont T**, **Kahán Z**, **Sárközy M.** Investigation of the antihypertrophic and antifibrotic effects of losartan in a rat model of radiation-induced heart disease. *Int J Mol Sci* 22: 12963, 2021. doi:10.3390/ijms222312963.
39. **Galla Z**, **Rácz G**, **Grecsó N**, **Baráth Á**, **Kósa M**, **Bereczki C**, **Monostori P.** Improved LC-MS/MS method for the determination of 42 neurologically and metabolically important molecules in urine. *J Chromatogr B Analyt Technol Biomed Life Sci* 1179: 122846, 2021. doi:10.1016/j.jchromb.2021.122846.
40. **Galla Z**, **Rajda C**, **Rácz G**, **Grecsó N**, **Baráth Á**, **Vécsei L**, **Bereczki C**, **Monostori P.** Simultaneous determination of 30 neurologically and metabolically important molecules: a sensitive and selective way to measure tyrosine and tryptophan pathway metabolites and other biomarkers in human serum and cerebrospinal fluid. *J Chromatogr A* 1635: 461775, 2021. doi:10.1016/j.chroma.2020.461775.
41. **Polyák H**, **Galla Z**, **Nánási N**, **Cseh EK**, **Rajda C**, **Veres G**, **Spekker E**, **Szabó Á**, **Klivényi P**, **Tanaka M**, **Vécsei L.** The tryptophan-kynurenine metabolic system is suppressed in cuprizone-induced model of demyelination simulating progressive multiple sclerosis. *Biomedicines* 11: 945, 2023. doi:10.3390/biomedicines11030945.
42. **Mody H**, **Vaidya TR**, **Ait-Oudhia S.** In vitro to clinical translational pharmacokinetic/pharmacodynamic modeling of doxorubicin (DOX) and dexrazoxane (DEX) interactions: safety assessment and optimization. *Sci Rep* 13: 3100, 2023. doi:10.1038/s41598-023-29964-4.
43. **Swain SM**, **Whaley FS**, **Ewer MS.** Congestive heart failure in patients treated with doxorubicin: a retrospective analysis of three trials. *Cancer* 97: 2869–2879, 2003. doi:10.1002/cncr.11407.
44. **Nebigil CG**, **Désaubry L.** Updates in anthracycline-mediated cardiotoxicity. *Front Pharmacol* 9: 1262, 2018. doi:10.3389/fphar.2018.01262.
45. **Lewandowski D**, **Yang EY**, **Nguyen DT**, **Khan MA**, **Malahfji M**, **El Tallawi C**, **Chamsi Pasha MA**, **Graviss EA**, **Shah DJ**, **Nagueh SF.** Relation of left ventricular diastolic function to global fibrosis burden: implications for heart failure risk stratification. *JACC Cardiovasc Imaging* 16: 783–796, 2023. doi:10.1016/j.jcmg.2022.12.027.
46. **Burlew BS**, **Weber KT.** Cardiac fibrosis as a cause of diastolic dysfunction. *Herz* 27: 92–98, 2002. doi:10.1007/s00059-002-2354-y.
47. **Zhan C**, **Bai N**, **Zheng M**, **Wang Y**, **Wang Y**, **Zhang L**, **Li J**, **Li G**, **Zhao H**, **Liu G**, **Lou Q**, **Yang W**, **Li T**, **Li L**, **Li W.** Tranilast prevents doxorubicin-induced myocardial hypertrophy and angiotensin II synthesis in rats. *Life Sci* 267: 118984, 2021. doi:10.1016/j.lfs.2020.118984.
48. **Pajović V**, **Kovácsházi C**, **Kosić M**, **Vasić M**, **Đukić L**, **Brenner GB**, **Giricz Z**, **Bajić D**, **Ferdinandy P**, **Japundžić-Žigon N.** Phenomapping for classification of doxorubicin-induced cardiomyopathy in rats. *Toxicol Appl Pharmacol* 423: 115579, 2021. doi:10.1016/j.taap.2021.115579.
49. **Lipshultz SE**, **Scully RE**, **Lipsitz SR**, **Sallan SE**, **Silverman LB**, **Miller TL**, **Barry EV**, **Asselin BL**, **Athale U**, **Clavell LA**, **Larsen E**, **Moghrabi A**, **Samson Y**, **Michon B**, **Schorin MA**, **Cohen HJ**, **Neuberg DS**, **Orav EJ**, **Colan SD.** Assessment of dexrazoxane as a cardioprotectant in doxorubicin-treated children with high-risk acute lymphoblastic leukaemia: long-term follow-up of a prospective, randomised, multicentre trial. *Lancet Oncol* 11: 950–961, 2010. doi:10.1016/S1470-2045(10)70204-7.

50. **Willis MS**, **Parry TL**, **Brown DI**, **Mota RI**, **Huang W**, **Beak JY**, **Sola M**, **Zhou C**, **Hicks ST**, **Caughey MC**, **D'Agostino RB**, **Jordan J**, **Hundley WG**, **Jensen BC.** Doxorubicin exposure causes subacute cardiac atrophy dependent on the striated muscle-specific ubiquitin ligase MuRF1. *Circ Heart Fail* 12: e005234, 2019. doi:10.1161/CIRCHEARTFAILURE.118.005234.
51. **Nakamura M**, **Sadoshima J.** Mechanisms of physiological and pathological cardiac hypertrophy. *Nat Rev Cardiol* 15: 387–407, 2018. doi:10.1038/s41569-018-0007-y.
52. **Kehat I**, **Molkentin JD.** Molecular pathways underlying cardiac remodeling during pathophysiological stimulation. *Circulation* 122: 2727–2735, 2010. doi:10.1161/CIRCULATIONAHA.110.942268.
53. **Phungphong S**, **Kijtawornrat A**, **Kampaengsri T**, **Wattanapermpool J**, **Bupha-Intr T.** Comparison of exercise training and estrogen supplementation on mast cell-mediated doxorubicin-induced cardiotoxicity. *Am J Physiol Regul Integr Comp Physiol* 318: R829–R842, 2020. doi:10.1152/ajpregu.00224.2019.
54. **Chen DS**, **Yan J**, **Yang PZ.** Cardiomyocyte atrophy, an underestimated contributor in doxorubicin-induced cardiotoxicity. *Front Cardiovasc Med* 9: 812578, 2022. doi:10.3389/fcvm.2022.812578.
55. **Sabapathy V**, **Cheru NT**, **Corey R**, **Mohammad S**, **Sharma R.** A novel hybrid cytokine IL233 mediates regeneration following doxorubicin-induced nephrotoxic injury. *Sci Rep* 9: 3215, 2019. doi:10.1038/s41598-019-39886-9.
56. **Watanabe M**, **Takimoto HR**, **Sasaki N.** Adriamycin-induced nephropathy models: elucidating CKD pathophysiology and advancing therapeutic strategies. *Exp Anim* 74: 132–142, 2025. doi:10.1538/expanim.24-0133.
57. **Quagliariello V**, **Berretta M**, **Bisceglia I**, **Giacobbe I**, **Iovine M**, **Barbato M**, **Maurea C**, **Canale ML**, **Paccone A**, **Inno A**, **Scherillo M**, **Oliva S**, **Cadeddu Dessalvi C**, **Mauriello A**, **Fonderico C**, **Maratea AC**, **Gabrielli D**, **Maurea N.** In the era of cardiovascular-kidney-metabolic syndrome in cardio-oncology: from pathogenesis to prevention and therapy. *Cancers (Basel)* 17: 1169, 2025. doi:10.3390/cancers17071169.
58. **Colak MC**, **Parlakpinar H**, **Tasdemir S**, **Samdanci E**, **Kose E**, **Polat A**, **Sarihan E**, **Acet A.** Therapeutic effects of ivabradine on hemodynamic parameters and cardiotoxicity induced by doxorubicin treatment in rat. *Hum Exp Toxicol* 31: 945–954, 2012. doi:10.1177/0960327112438288.
59. **Boeno FP**, **Patel J**, **Montalvo RN**, **Lapierre-Nguyen SS**, **Schreiber CM**, **Smuder AJ.** Effects of exercise preconditioning on doxorubicin-induced liver and kidney toxicity in male and female rats. *Int J Mol Sci* 24: 10222, 2023. doi:10.3390/ijms241210222.
60. **Grant MKO**, **Seelig DM**, **Sharkey LC**, **Choi WSV**, **Abdelgawad IY**, **Zordoky BN.** Sexual dimorphism of acute doxorubicin-induced nephrotoxicity in C57Bl/6 mice. *PLoS One* 14: e0212486, 2019. doi:10.1371/journal.pone.0212486.
61. **Zordoky BN**, **Radin MJ**, **Heller L**, **Tobias A**, **Matise I**, **Apple FS**, **McCune SA**, **Sharkey LC.** The interplay between genetic background and sexual dimorphism of doxorubicin-induced cardiotoxicity. *Cardiooncology* 2: 4, 2016. doi:10.1186/s40959-016-0013-3.
62. **Rangaswami J**, **Bhalla V**, **Blair JEA**, **Chang TI**, **Costa S**, **Lentine KL**, **Lerma EV**, **Mezue K**, **Molitch M**, **Mullens W**, **Ronco C**, **Tang WHW**, **McCullough PA**; **American Heart Association Council on the Kidney in Cardiovascular Disease and Council on Clinical Cardiology.** Cardiorenal syndrome: classification, pathophysiology, diagnosis, and treatment strategies: a scientific statement from the American Heart Association. *Circulation* 139: e840–e878, 2019. doi:10.1161/CIR.0000000000000664.
63. **Rubin JB**, **Lagas JS**, **Broestl L**, **Sponagel J**, **Rockwell N**, **Rhee G**, **Rosen SF**, **Chen S**, **Klein RS**, **Imoukhuede P**, **Luo J.** Sex differences in cancer mechanisms. *Biol Sex Differ* 11: 17, 2020. doi:10.1186/s13293-020-00291-x.
64. **Shahzadi A**, **Eyileten C**, **Postula M**, **Tanoglu EG**, **Karatas OF**, **Basci AB**, **Suzer O**, **Yazici Z.** Investigation of doxorubicin combined with ciprofloxacin-induced cardiotoxicity: from molecular mechanism to fundamental heart function. *Naunyn Schmiedebergs Arch Pharmacol* 396: 1547–1561, 2023. doi:10.1007/s00210-022-02331-2.
65. **Grant MKO**, **Seelig DM**, **Sharkey LC**, **Zordoky BN.** Sex-dependent alteration of cardiac cytochrome P450 gene expression by doxorubicin in C57Bl/6 mice. *Biol Sex Differ* 8: 1, 2017. doi:10.1186/s13293-016-0124-4.
66. **Bagdasaryan AA**, **Chubarev VN**, **Smolyarchuk EA**, **Drozdov VN**, **Krasnyuk II**, **Liu J**, **Fan R**, **Tse E**, **Shikh EV**, **Sukocheva OA.** Pharmacogenetics of drug metabolism: the role of gene polymorphism in the regulation of doxorubicin safety and efficacy. *Cancers (Basel)* 14: 5436, 2022. doi:10.3390/cancers14215436.
67. **Shakeri H**, **Boen JRA**, **De Moudt S**, **Hendrickx JO**, **Leloup AJA**, **Jacobs G**, **De Meyer GRY**, **De Keulenaer GW**, **Guns PDF**, **Segers VFM.** Neuregulin-1 compensates for endothelial nitric oxide synthase deficiency. *Am J Physiol Heart Circ Physiol* 320: H2416–H2428, 2021. doi:10.1152/ajpheart.00914.2020.
68. **Janssens S**, **Pokreisz P**, **Schoonjans L**, **Pellens M**, **Vermeersch P**, **Tjwa M**, **Jans P**, **Scherrer-Crosbie M**, **Picard MH**, **Szelid Z**, **Gillijns H**, **van de Werf F**, **Collen D**, **Bloch KD.** Cardiomyocyte-specific overexpression of nitric oxide synthase 3 improves left ventricular performance and reduces compensatory hypertrophy after myocardial infarction. *Circ Res* 94: 1256–1262, 2004. doi:10.1161/01.RES.0000126497.38281.23.
69. **Wu W**, **Yang B**, **Qiao Y**, **Zhou Q**, **He H**, **He M.** Kaempferol protects mitochondria and alleviates damages against endotheliotoxicity induced by doxorubicin. *Biomed Pharmacother* 126: 110040, 2020. doi:10.1016/j.biopha.2020.110040.
70. **Finkelman BS**, **Putt M**, **Wang T**, **Wang L**, **Narayan H**, **Domchek S**, **DeMichele A**, **Fox K**, **Matro J**, **Shah P**, **Clark A**, **Bradbury A**, **Narayan V**, **Carver JR**, **Tang WHW**, **Ky B.** Arginine-nitric oxide metabolites and cardiac dysfunction in patients with breast cancer. *J Am Coll Cardiol* 70: 152–162, 2017 [Erratum in *J Am Coll Cardiol* 70: 2738, 2017]. doi:10.1016/j.jacc.2017.10.041.
71. **Riddell A**, **Flynn A**, **Bergugnat H**, **Dowsett LB**, **Miller AA.** SDMA as a marker and mediator in cerebrovascular disease. *Clin Sci (Lond)* 138: 1305–1323, 2024. doi:10.1042/CS20241021.
72. **McCarty MF.** Asymmetric dimethylarginine is a well established mediating risk factor for cardiovascular morbidity and mortality-should patients with elevated levels be supplemented with citrulline? *Healthcare (Basel)* 4: 40, 2016. doi:10.3390/healthcare4030040.
73. **Guo X**, **Xing Y**, **Jin W.** Role of ADMA in the pathogenesis of microvascular complications in type 2 diabetes mellitus. *Front Endocrinol (Lausanne)* 14: 1183586, 2023. doi:10.3389/fendo.2023.1183586.
74. **Pan W**, **Lian B**, **Lu H**, **Liao P**, **Guo L**, **Zhang M.** Prognostic value of asymmetric dimethylarginine in patients with heart failure: a systematic review and meta-analysis. *Biomed Res Int* 2020: 6960107, 2020. doi:10.1155/2020/6960107.
75. **Heiss EH**, **Dirsch VM.** Regulation of eNOS enzyme activity by post-translational modification. *Curr Pharm Des* 20: 3503–3513, 2014. doi:10.2174/13816128113196660745.
76. **Janaszak-Jasiecka A**, **Płoska A**, **Wierońska JM**, **Dobrucki LW**, **Kalinowski L.** Endothelial dysfunction due to eNOS uncoupling: molecular mechanisms as potential therapeutic targets. *Cell Mol Biol Lett* 28: 21, 2023. doi:10.1186/s11658-023-00423-2.
77. **Garcia V**, **Sessa WC.** Endothelial NOS: perspective and recent developments. *Br J Pharmacol* 176: 189–196, 2019. doi:10.1111/bph.14522.
78. **Octavia Y**, **Kararigas G**, **Mde BOER**, **Chrifi I**, **Kietadisorn R**, **Swinnen M**, **Duimel H**, **Verheyen FK**, **Brandt MM**, **Fliegner D**, **Cheng C**, **Janssens S**, **Duncker DJ**, **Moens AL.** Folic acid reduces doxorubicin-induced cardiomyopathy by modulating endothelial nitric oxide synthase. *J Cell Mol Med* 21: 3277–3287, 2017. doi:10.1111/jcmm.13231.
79. **Schnackenberg LK**, **Pence L**, **Vijay V**, **Moland CL**, **George N**, **Cao Z**, **Yu L-R**, **Fuscoe JC**, **Beger RD**, **Desai VG.** Early metabolomics changes in heart and plasma during chronic doxorubicin treatment in B6C3F1 mice. *J Appl Toxicol* 36: 1486–1495, 2016. doi:10.1002/jat.3307.
80. **Mor A**, **Kalaska B**, **Pawlak D.** Kynurenine pathway in chronic kidney disease: what's old, what's new, and what's next? *Int J Tryptophan Res* 13: 1178646920954882, 2020. doi:10.1177/1178646920954882.
81. **Li D**, **Zhang Y**, **Kuang Y**, **Lin Z**, **Wang P**, **Jiang J**, **Pi W**, **Ma Q.** Reprogramming of the kynurenine pathway impairs NAD^+ homeostasis and mediates doxorubicin-induced cardiotoxicity in mice. *Redox Biol* 89: 103957, 2026. doi:10.1016/j.redox.2025.103957.
82. **Mobasheran P**, **Aguilar J**, **Aryal A**, **Jennings S**, **Xia H**, **Yang Q.** Abstract Fri080: kynurenic acid mitigates doxorubicin-cardiomyopathy via improving mitochondrial function and silencing ATP synthase inhibitory subunit 1 (Abstract). *Circ Res* 137, 2025. doi:10.1161/res.137.suppl_1.Fri080.

83. **Zhang Y**, **Ying F**, **Tian X**, **Lei Z**, **Li X**, **Lo CY**, **Li J**, **Jiang L**, **Yao X.** TRPM2 promotes atherosclerotic progression in a mouse model of atherosclerosis. *Cells* 11: 1423, 2022. doi:10.3390/cells11091423.
84. **Benitez T**, **VanDerWoude E**, **Han Y**, **Byun J**, **Konje VC**, **Gillespie BW**, **Saran R**, **Mathew AV.** Kynurenine pathway metabolites predict subclinical atherosclerotic disease and new cardiovascular events in chronic kidney disease. *Clin Kidney J* 15: 1952–1965, 2022. doi:10.1093/ckj/sfac138.
85. **Choi J-W**, **Aseer KR**, **Chaudhari HN**, **Mukherjee R**, **Choi M**, **Yun JW.** Gender dimorphism in regulation of plasma proteins in streptozotocin-induced diabetic rats. *Proteomics* 13: 2482–2494, 2013. doi:10.1002/pmic.201200529.
86. **Mor A**, **Tankiewicz-Kwedlo A**, **Krupa A**, **Pawlak D.** Role of kynurenine pathway in oxidative stress during neurodegenerative disorders. *Cells* 10: 1603, 2021. doi:10.3390/cells10071603.
87. **Lopaschuk GD**, **Karwi QG**, **Tian R**, **Wende AR**, **Abel ED.** Cardiac energy metabolism in heart failure. *Circ Res* 128: 1487–1513, 2021. doi:10.1161/CIRCRESAHA.121.318241.
88. **Zhou P**, **Pu WT.** Recounting cardiac cellular composition. *Circ Res* 118: 368–370, 2016. doi:10.1161/CIRCRESAHA.116.308139.
89. **Chen S**, **Zou Y**, **Song C**, **Cao K**, **Cai K**, **Wu Y**, **Zhang Z**, **Geng D**, **Sun W**, **Ouyang N**, **Zhang N**, **Li Z**, **Sun G**, **Zhang Y**, **Sun Y**, **Zhang Y.** The role of glycolytic metabolic pathways in cardiovascular disease and potential therapeutic approaches. *Basic Res Cardiol* 118: 48, 2023. doi:10.1007/s00395-023-01018-w.
90. **Shao D**, **Tian R.** Glucose transporters in cardiac metabolism and hypertrophy. *Compr Physiol* 6: 331–351, 2015. doi:10.1002/cphy.c150016.
91. **Russo M**, **Della Sala A**, **Tocchetti CG**, **Porporato PE**, **Ghigo A.** Metabolic aspects of anthracycline cardiotoxicity. *Curr Treat Options Oncol* 22: 18, 2021. doi:10.1007/s11864-020-00812-1.
92. **Zhang L**, **Jaswal JS**, **Ussher JR**, **Sankaralingam S**, **Wagg C**, **Zaugg M**, **Lopaschuk GD.** Cardiac insulin-resistance and decreased mitochondrial energy production precede the development of systolic heart failure after pressure-overload hypertrophy. *Circ Heart Fail* 6: 1039–1048, 2013. doi:10.1161/CIRCHEARTFAILURE.112.000228.
93. **Arunachalam S**, **Tirupathi Pichiah PB**, **Achiraman S.** Doxorubicin treatment inhibits PPARγ and may induce lipotoxicity by mimicking a type 2 diabetes-like condition in rodent models. *FEBS Lett* 587: 105–110, 2013. doi:10.1016/j.febslet.2012.11.019.